Background stratification impacts on internal tides generation and abyssal propagation in the Western Equatorial Atlantic and the Bay of Biscay

Simon Barbot[1], Florent Lyard[1], Michel Tchilibou[1], and Loren Carrere[2]

[1]LEGOS, Université de Toulouse, CNES, CNRS, IRD, UPS, Toulouse, France
[2]CLS, Ramonville-Saint-Agne, France

Correspondence: Simon Barbot (simon.barbot@legos.obs-mip.fr)

Abstract. The forthcoming SWOT altimetric mission aims to access the smaller mesoscale oceanic circulation with an unprecedented spatial resolution and swath. The repetitivity of the mission orbit implies that high frequency processes, such as the internal tides (ITs), are under-sampled in time and their full temporal evolution is not observed. They are therefore aliased onto lower frequencies and possibly mixed into the mesoscale signals. As with the barotropic tides, the ITs must be corrected from the altimetric observations in order to access to the smaller mesoscales. But unlike barotropic tides, ITs are not completely stationary and have significant temporal variability due to their interactions with the ocean circulation and the stratification variability. ITs prediction, correction and error calculation requires a precise understanding of the ITs' surface elevation signature and its temporal variability. Stratification changes impact both on the generation and the propagation of ITs. This present study proposes to quantify the impacts of the background stratification variations alone with a classification of the observed stratification and an idealized modeling of the ITs. A single methodology is developed to handle a very broad range of stratification variability. The classification is made using clustering methods and the modeling uses the frequency domain model T-UGO.

The methodology is successfully tested on the western equatorial Atlantic and in the Bay of Biscay. For the western equatorial Atlantic, the pycnocline depth linearly impacts on the amplitudes and wavelengths of the ITs first two modes. An increase of the pycnocline depth increases the total ITs' amplitude but also transfers the energy from mode 2 to mode 1. An increase of the pycnocline depth also increases the wavelengths of both modes 1 and 2. In the Bay of Biscay we found no such proxy to describe the changes in ITs' characteristics so a seasonal climatology is explored. The seasonality of the stratification strongly affects the amplitudes of modes 2 and 3 and significantly impacts on the surface elevation of ITs. Whereas the wavelengths of all modes and the amplitude of mode 1 are only weakly affected by the stratification seasonality. The amplitude variability of modes 2 and 3 also modifies the ratio between the modes in presence and makes the horizontal scales of ITs variable. The significance of the ITs wavelength modifications with stratification changes suggests that a more accurate ITs' surface elevation correction for SWOT measurements should take into account this stratification variability.

1 Introduction

Internal tides (ITs) are internal waves with tidal frequency. ITs are generated when the energy fluxes of the barotropic tide are
perpendicular to a bathymetric slope within a stratified ocean. The vertical oscillations produced interact with non-tidal ocean
circulation and enhance the vertical mixing of the ocean. The generation and propagation of ITs are modulated by the ocean
circulation, especially the mesoscale dynamics, but also by the stratification variability. Thus, contrary to barotropic tides, the
sensitivity of the ITs to the ocean conditions is responsible for a significant temporal variability of their harmonic amplitude
and phase.

The studies of Ray and Mitchum (1996, 1997), first around Hawaiian islands and then globally, were the first to observe
ITs from altimetric time series using harmonic analysis. Thier method highlighted that the surface elevation due to ITs had a
stationary signature over the 4 years of measurements. Ever since, the ITs' surface elevation has been separated into stationary
(or coherent, or phase-locked in the literature) and non-stationary (or incoherent). The non-stationarity of the ITs is due to the
temporal variability of the ocean conditions impacting the ITs' generation and propagation. The ITW' generation is impacted
by the stratification changes due to radiative forcing or ocean circulation changes and by the variability of the barotropic tidal
forcing. The ITs' propagation pathway is also impacted by such stratification modifications as well as circulation processes
such as geostrophic currents (*e.i* Pereira et al., 2007 for realistic approach ; *e.i* Chuang and Wang, 1981 for idealized approach)
and eddies (*e.i* Duda et al., 2018 for realistic approach ; *e.i* Ponte and Klein, 2015 for idealized approach) that directly interact
with the ITs. With the increase in the altimetric time series, global maps of the stationary ITs' surface elevation amplitude
become more precise (Carrere et al., 2004; Ray and Zaron, 2016; Zaron, 2019; Zhao et al., 2019; Carrere et al., 2021). Based
on the residuals of these global maps, Zaron and Ray (2017) evaluated the non-stationary amplitude. The authors highlight that
most of the tropics are dominated by non-stationary ITs.

The forthcoming SWOT satellite mission (Morrow et al., 2019) is designed to observe the fine scale 2D elevation of the
continental waters as well as sea surface height (SSH). Global measurements will be made along two 50 km wide swaths
in addition to the traditional nadir measurements. During its nominal phase, SWOT's wide-swath coverage will be repeated
every 20.86 days for at least 3 years (Fu and Ubelmann, 2014). This orbit was carefully selected to separate the main tidal
constituents after 3-years. For the ocean, two products with a resolution of 2 km and 250 m should be available in the open
and coastal oceans[1]. This wide-swath measurement pattern will allow us to access the fine scale SSH and, for the first time,
observe the smaller mesoscale circulation and ITs in 2D (processes from 150 km to 15 km).

Such spatial resolution enables us to detect the ITs but the poorer temporal resolution prevents them from being properly
resolved in frequency space. The high frequency signals of the ITs are aliased into lower frequencies, within the range of
mesoscale and sub-mesoscale processes. For instance, the aliased period of the main three tidal constituents for SWOT will
be about 66 days for the M2 tides, about 77 days for the S2 tides and about 266 days for the K1 tides (for T/P : 62 days for
M2, 58 days for S2 and 270 days for K1). ITs' SSH wavelengths are also in a similar range as the typical spatial scales of
mesoscale and sub-mesoscale circulations. It is important to separate the aliased barotropic tides and ITs signals from the SSH

---

[1]https://podaac.jpl.nasa.gov/SWOT?tab=datasets§ions=about

before calculating geostrophic currents or vorticity, since the tide signals are not in geostrophic balance. Yet the overlap in spatial and temporal variability between ITs and the mesoscales creates a complex separation issue. In harmonic analysis from altimetry observations, the contamination of tidal signal by non-tidal ones generally diminishes as the observation duration increases. For quasi-stationary tides (such as barotropic tides), this means that the accuracy of the tidal harmonics improves with time. However, for ITs, the proportion of the stationary component, captured by the harmonic analysis, in the total ITs' SSH diminishes as the observation duration increases due to the increased ocean variability over time. So empirical ITs corrections, are either inaccurate if based on short observation periods (stationary part issue) or incomplete if based on long observation period (non-stationary part issue).

The SWOT measurements cumulate two factors: an inappropriate space-time sampling to resolve ITs and the non-stationarity of the ITs themselves (Arbic et al., 2015). The interlaced space-time spectrum of ITs and mesoscale circulation in the SWOT observations advocate for producing the best possible ITs correction and then quantifying the ITs' residuals that will not be corrected. For these reasons an international effort is taking place in order to propose new methods of ITs detection in SWOT observations (*e.i.* Zhao et al., 2018) and increase the knowledge on ITs' non-stationarity (*e.i.* Tchilibou et al., 2019). The present study aims at contributing to the understanding of the ITs' non-stationarity through the investigation of the ITs variability.

Here, one of the key factor of the ITs generation and propagation is investigated: the stratification and its temporal variability. A dual approach will be used based on the classification of observations and ITs modeling. The classification will help us to characterize the stratification variability. The ITs modeling will enable us to quantify the impacts of such stratification variability on the ITs' SSH. Such idealized simulations are interesting to explore the ITWs properties, before running more realistic but complex 3D simulations. This methodology will be tested in two areas where the stratification variability is driven by different processes.

After brief reminders about ITs and the stratification in section 2, the present study is divided into two main parts. Section 3 addresses the usage of the clustering methods, the different methods and the different configurations investigated. The classification of each area will be discussed and compared to the equivalent three-month mean. Section 4 addresses the modeling of the ITs based on the typical profiles. An academic configuration of the T-UGOm, a frequency domain model, is used for each typical stratification profile. The evolution of the surface elevation amplitude and wavelength will be extracted from the simulations and some climatologies will be proposed. The results for the western equatorial Atlantic will be compared to the regional simulation of Ruault et al. (2020) and the altimetric ITs map of Zaron (2019). This organisation enables to better compare how the presented methodology can handle the two areas that have two different stratification variabilities.

2 Background knowledge

2.1 ITs' dependency to stratification

The stratification controls the buoyancy of the water masses that is the restoring force of the internal waves. Starting from a stratified ocean at rest, with horizontal isopycnals, the vertical displacement of a given layer at some position will create a horizontal baroclinic pressure gradient. This will propagate as an internal gravity wave. Stronger stratification will generate
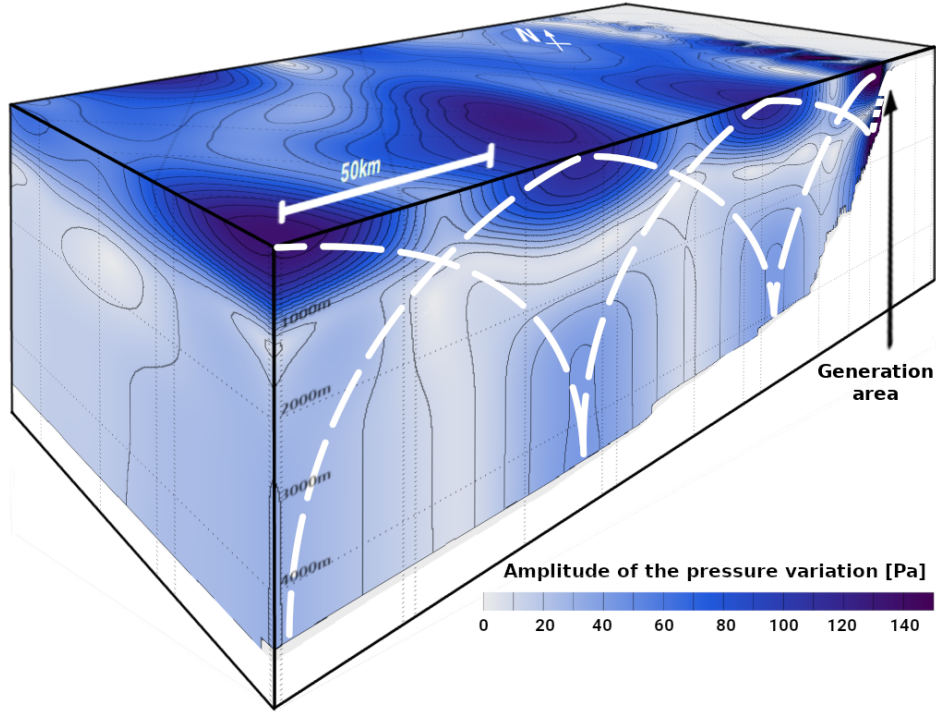
Figure 1. 3D visualisation of the internal tides (ITs) signature on the pressure amplitude. The white dashed lines represent the wave beam of the ITs.

stronger internal gravity waves. In the case of ITs, the vertical displacements occur when the periodic, barotropic (horizontal) tidal flow is oriented across a topographic slope. In a finite depth ocean, assuming that hydrostatic approximation holds, the ITs vertical wavenumbers are constrained by the depth. Those wavenumbers can be developed in different vertical modes for each permitted vertical wavenumber. In a continuously stratified ocean, the number of modes can be infinite. In a two-layer ocean, only one baroclinic vertical mode is supported. In a numerical model, the number of modes will be limited by the number of layers in the model grid.

Stratification is characterized by the Brunt-Väissälä frequency N (Gill, 1982):

$$N^2 = -\frac{g}{\rho_0}\frac{d\rho_0}{dz} \tag{1}$$

with g the gravitational acceleration, ρ_0 the unperturbed potential density. N is one of the governing terms of the linear internal wave theory that accounts for the velocity and pressure perturbations in the vertical equations. In practice, the vertical profile of N will dictate the partition of energy between the various modes (mostly concentrated in the first ones). Each mode has a specific horizontal wavenumber associated with its vertical wavenumber through the dispersion relationship (internal gravity wave in a rotating fluid Kundu et al., 2004):

$$\omega^2 - N^2\frac{k_H^2}{k_H^2 + k_V^2} + f^2\frac{k_V^2}{k_H^2 + k_V^2} = 0 \tag{2}$$

with f the Coriolis parameter, ω the wave frequency, k_H the horizontal wavenumber and k_V the vertical wavenumber.

The variety of horizontal wavelengths results in a field of constructive and destructive interactions between the various modes composing the physical internal wave. The ITs' final signature is illustrated by Figure 1: where the amplitude is high, the modes interactions are constructive; where the amplitude is low, the modes interactions are destructive. The pathway of high amplitude supports the energy flux of the ITs and is called the wave beam (white dashed lines on Figure 1).

Being waves, the ITs are sensitive to the density of the field they are propagating through. Spatial variability of the density causes the refraction and reflection of the waves. The ITs slope a in the water column (equivalent to the slope of the wave beam) is defined by the ratio between horizontal and vertical wavenumber, from the Equation 2 this leads to:

$$a^2 = \frac{k_H^2}{k_V^2} = \frac{\omega^2 - f^2}{N^2 - \omega^2} \tag{3}$$

Because N depends on the depth, the vertical profile of N implies a vertical profile of a as well. The variation of a with depth explain the wave beam shape, like a Gothic vault. The surface elevation of the ITs directly depends on the value of a throughout the water column as well as the ocean depth. As shown in Figure 1, the distance between two maximums of surface elevation is related to the wave beam pathway. Thus, the stratification and the depth both impact the horizontal wavelength of the ITs during its propagation.

The stratification is thus one of the controlling term of the intensity and horizontal patterns of the ITs' generation and propagation. The goal of the present study is to quantify the impacts of the stratification variations on ITs' characteristics. The impact on the generation is monitored by the amplitude. The impact on the propagation is monitored by the horizontal wavelength. Before investigating these impacts, we will discuss the range of stratification variability that needs to be investigated.

2.2 Stratification variability

Two main processes control the stratification variability in the ocean. The first one is the radiative forcing from the Sun that heats up the surface layers. The seasonality of this process is weaker in the tropics than at mid or high latitudes. The second one is the mixing of water masses induced by the circulation. The variability of the circulation has multiple timescales: away from strong currents, the circulation at intermediate and deep depths is almost stationary, and the circulation at the surface is highly variable at seasonal to shorter timescales.

In addition of the stratification, the currents also affect the ITs propagation and complexify the ITs signal. The investigation of such dynamical impacts over ITs is beyond the scope of this study. Here, the stratification is investigated without background current in order to only quantify the ITs signal response to the stratification alone. Such stratification is further named background stratification. Such stratification is further named *background stratification*.

Two areas of interest have been chosen for their very different stratification variability and strong ITs generation. The western equatorial Atlantic is well known to be dominated by non-stationary ITs signature (Magalhães et al., 2016; Zaron and Ray, 2017). Located at the equator, the stratification is dominated by the circulation rather than the radiative forcing. The recent regional simulation of Ruault et al. (2020) will be used to validate the results. The Bay of Biscay is one of the most studied ITs generation areas. Located in the mid-latitudes and with weak ocean circulation, the stratification variability is dominated

by the radiative forcing. The variability of the background stratification is investigated by making realistic classifications of stratification profiles from *in situ* measurements. Then, each class provides a typical stratification profile.

A common way to classify the background stratification is to make four seasonal means (based on the mean of three months ; further named three-month means) or monthly means. Such a method is easy to use but affects the realism of the profiles. The temporal mean erases the extremums of the profiles, does not consider spatial variability of the area and vertically smooths the profiles. Using different boxes within an area and using a small time interval can increase the realism of the profiles but leads to processing of a huge number of mean profiles (further named typical profiles). To maintain the realism of the typical profiles with only a few of them, the profiles are classified using clustering methods.

The clustering methods are based on the similarity of the profiles with each other to calculate an optimal classification. They are used in many different disciplines (from sociology and biology to economics and astrophysics) and start to be applied on the ocean's physical properties. In the last years, they have been applied to improve temperature and salinity climatologies (Hjelmervik and Hjelmervik, 2013, 2014), to track water masses (Martin Traykovski and Sosik, 2003; Oliver et al., 2004), to study the evolution of the oceanic desert areas (Irwin and Oliver, 2009) or identify the impact of eddies on the water masses (Pegliasco et al., 2015). These methods can handle spatio-temporal variability and can highlight the potential patterns of the extremum profiles.

3 The classification of the density profiles

3.1 Data

To study the variability of the density profiles, the CORA dataset is used (Coriolis Ocean Dataset for Reanalysis; Szekely et al., 2016 provided by Copernicus monitoring service[2] and SEANOE; SEA scieNtific Open data Edition[3]). Different versions are available but the latest versions (>5.0) are reprocessed data and provide only monthly-averaged data. In order to get a larger number of profiles, the quality controlled data compiled in the version 4.3 is used. This version gathers all kinds of measurements in the ocean sorted by date and instrument. Because density is targeted, only the instruments that measure profiles of temperature and salinity at the same time are selected: Argo float, CTD, XCTD and moorings. The areas of interest are defined as follows: for the western equatorial Atlantic, from 5°S to 15°N and from 60°W to 35°W; for the Bay of Biscay, from 43°N to 48.5°N and from 10°W to 0°W (Fig. 2b,d). These individual profiles are used for the cluster analysis.

The typical density profiles derived from the clusters are compared to common three-month mean, averaged over the two areas of interest and processed from the same dataset. In addition the clusters are compared to existing climatologies, also averaged over the two areas. For the Bay of Biscay, BOBYCLIM is used (Bay Of BiscaY's CLIMatology ; Charraudeau, 2006 ; produced by the Ifremer [4]). This seasonal climatology uses the profiles in this area from 1862 to 2006 classified into four seasons (three-month means), using a grid of $1/5^{th}$ of degree. For both the western equatorial Atlantic and the Bay of Biscay,

---

[2]http://marine.copernicus.eu/

[3]https://www.seanoe.org/

[4]http://www.ifremer.fr/climatologie-gascogne/climatologie/index.php
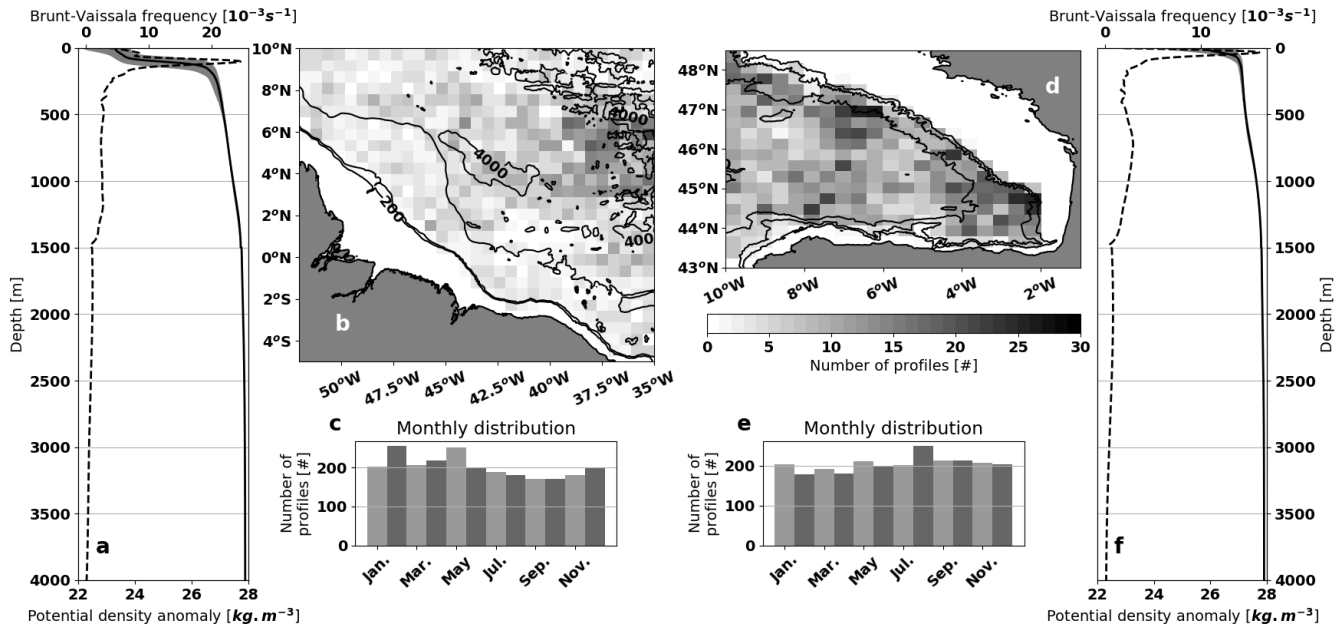
Figure 2. Characteristics of the *in situ* density profiles in the CORA V4.3 dataset for the two areas of interest: (a,b,c) the western equatorial Atlantic and (d,e,f) the Bay of Biscay. (b,d) present the spatial distribution the profiles within boxes of 60 kmx60 km for (b) and 30 kmx30 km for (d). (c,e) present the monthly distribution of the profiles. (a,f) present the mean (solid line) and the 90% interval (grey patch) of the density profiles as well as the Brunt-Väissälä profiles (dash line).

ISAS13 climatology is used (*In-Situ* Analysis System ; Gaillard, 2015 ; provided by Copernicus and SEANOE). This monthly climatology is based on the CORA database and averaged from 2004 to 2014, using a grid of $1/5^{th}$ of degree. The seasonal climatology of ISAS13 is built using three-month means. As the radiative forcing is weak in the western equatorial Atlantic, the annual climatology is also build by averaging all the months.

170   Whatever the data, the potential density is calculated. The potential density is the density of the water that is adiabatically brought back to a reference pressure. This is equivalent to computing the density using the potential temperature instead of the *in situ* one. This convention removes the effect of the pressure on the density. Note that the potential density is responsible for the restoring forces and is used in the definition of N (Eq. 1). The TEOS-10 convention (Millero et al., 2008) that uses the Gibbs Sea Water (GSW) equations of Feistel (2003, 2008) is used to calculate the potential density of the profiles (Python

175   GSW package[5]).

Figure 2 presents the distribution of the dataset for both areas of interest. For the western equatorial Atlantic area, the density profiles (Fig. 2a) are strongly stratified around 100 m. Most of the variability of the profiles is around this depth but also at the surface, mainly due to the variability of the North Brazil Current (NBC, Garraffo et al., 2003). The surface variability is also due to the Amazon river plume and the variability of the river discharge (Ffield, 2005). Then the stratification remains constant

---

[5]https://github.com/TEOS-10/python-gsw

down to 1500 m and slightly decreases close to the bottom. Note that the spatial distribution of the profiles is not homogeneous, less profiles being available along the shelf break. In the Bay of Biscay area, the density profiles (Fig. 2f) are less stratified than for the western equatorial Atlantic. The strongest stratification and the largest variability occurs at the surface. This pattern expresses the dominance of the radiative forcing in this region. Around 700 m, another stratification maximum can be observed. This particular pattern is present in the study of Pichon and Correard (2006) and further detailed in Pairaud et al. (2010). The spatial distribution of the profiles is quite homogeneous in this region.

3.2 Methodology of the classification

3.2.1 Pre-processing of the data

The variability of the ocean stratification is dominated by the surface density variations (Fig. 2a,d). Hence, in this section, the profiles are selected and processed only for the surface layer, which is defined with respect to the variability of the profiles: above 300 m in the Bay of Biscay, above 600 m in the western equatorial Atlantic. Since the measurements have more uncertainties at the surface, the top limit of the working layer is set to 10 m.

The typical density profiles will be used in a frequency-domain tidal model (see section 4.1). Hence, only the stable density profiles are processed. The measurements can still be noisy (presenting a negative density gradient) without presenting unstable water masses. The threshold used to define an unstable profile is when there are more than two consecutive occurrences of $\delta_z \rho < -0.5$ kg.m^{-4} (with $\delta_z \rho$ the vertical density gradient).

Focusing on the stratification sampling interval, the profiles need to have a sufficient vertical resolution. The selected profiles must have more than 5 measurements over 100 m inside the surface layer. In order to run the algorithms faster, the profiles need to be on the same vertical grid and without any missing values. Thus, the density profiles are linearly interpolated to fill all the gaps and get all the profiles on a vertical grid of 1 m resolution.

Now that the profiles are properly selected and interpolated, the shape of each profile needs to defined within a two co-ordinates system in order to calculate the distance between each other. For that purpose, the profiles are processed using the principal component analysis (PCA; Python SciKitLearn decomposition package[6]) following a similar procedure as Pauthenet et al. (2018) in their temperature profile study within Southern Ocean fronts.

As the profiles are only described by the density versus depth, only two principal components are used. Thus, the shape of each profile is evaluated according to two orthogonal axes. The PCA manifold is the plan defined by these two new axes and where each profile is characterized by a point. The both axes explain a different part of the standard deviation of the profiles. For example, if the profiles are mainly controlled by the pycnocline depth but also by the surface density, the first axis (PC1) will be controlled by the different depths of the pycnocline whereas the second axis (PC2) will be controlled by the surface depths. The clustering method classifies the profiles within the PCA manifold by calculating the distance from one point to every other points, minimizing the distance within each cluster. Once the classification is made within this artificial space, the classification can be applied to the density profiles back on a physical space.

---

[6]https://scikit-learn.org/stable/modules/decomposition.html

The distribution within the PCA manifold can be improved by normalizing the profiles before performing the PCA. But as expressed in Equation 3, the ITs wave beam slope a is a function of N that is directly affected by the value of the density ρ_0 in addition to the vertical gradient of ρ_0 (Eq. 1). So the ITs are directly affected by the values of the density profile, not only the shape of the profile. Hence, in order to keep the entire information of the profiles, the profiles are classified without using any normalization.

3.2.2 Parameters controlling the clustering methods

Three methods of clustering are compared: Ward, Average and Spectral (Python SciKitLearn clustering package[7]). Those methods have been selected because they can better classify similar PCA manifold that we have Fig. A1). For each method, the sensitivity of two parameters needs to be investigated: the number of final clusters and the number of neighbors used in the calculation of the distance between profiles. The number of neighbors is important to properly manage the profiles that are isolated outside the PCA manifold. If the number of neighbors is weaker than the number of outsider profiles, then they all would be grouped in a dedicated cluster. Otherwise, they would be included in the cluster of the nearest profiles. This latter case can lead to groups of profiles that do not have the same shape inside the same cluster. The number of neighbors also affects the profiles located at the boundary between two clusters: depending on the number of neighbors, they would be included in one cluster or another.

A wide range of sensitivity tests have been made to choose the best method and the best parameters. The number of neighbors is tested from 4 to 16 and the number of clusters is tested from 2 to 10. These results can be found in the appendix A. The Ward method is used in the rest of the study because it offers a wider range of stratification cases and it is less sensitive to the number of neighbors. The classifications using the 16 nearest neighbors are distributed more equally between the clusters so this parameter is chosen. The number of clusters is set more arbitrarily. For the western equatorial Atlantic, the variability of the density profiles is controlled by the pycnocline depth with almost no modification of the N profile. Thus, few clusters are needed to characterize such variability. For the Bay of Biscay, the variability of the density profiles is way more complex and N profiles are very different even for 10 clusters. But a high number of clusters leads to have some clusters with few profiles. Thus, for both areas, a classification of 6 clusters is a good compromise that enables us to detail the evolution of the density profiles while keeping well represented clusters (more than 100 profiles).

3.2.3 Post-processing of the clusters for modeling purpose

Once the classification is done, the typical profile from each cluster is calculated in order to use it as a forcing in the simulations (see section 4.1). The density profiles need to be strictly stable and defined from 0 to 4000 m depth.

Because most of the profiles used for the classification are not defined that deep, the completion process is detailed here. The median of the profiles within the clusters is used as deep as possible. The standard deviation below 1000 m is very weak (Fig. 2a,f) so the profile can be completed with the median of the profiles from the other clusters. If the profile does not reach 4000

---

[7]https://scikit-learn.org/stable/modules/clustering.html

Table 1. Composition of the clusters and the characteristics of their stratification maximum for the western equatorial Atlantic and the Bay of Biscay. The depth of $N_{\max}$ corresponds to the pycnocline depth.

Cluster	western equatorial Atlantic (WEA)			Bay of Biscay (BB)		
	Profiles	$N_{\max}$	Depth $N_{\max}$	Profiles	$N_{\max}$	Depth $N_{\max}$
#	#	$[[10^{-3}\,\mathrm{s}^{-1}]$	[m]	#	$[10^{-3}\,\mathrm{s}^{-1}]$	[m]
1	628	25.7	72	787	4.0	133
2	576	22.6	108	424	11.3	35
3	528	23.7	88	419	7.2	45
4	336	23.9	128	324	19.9	35
5	336	23.8	148	316	19.3	35
6	17	NA	NA	177	15.9	30
Mean	-	23.9	106	-	15.2	52
Total	2421	-	-	2447	-	-

m, then the bottom of the profile is extrapolated using the density gradient of the latest 4 measurements. The density gradient used for the extrapolation needs to be weaker than $5.0 \cdot 10^{-7}\,\mathrm{kg.m}^{-4}$ that is a common gradient at such a deep depth.

245   The median profiles have been smoothed using several forward-backward filters (Python SciPy signal package[8]). Many trials have been made to have the smoothest profiles while keeping most of the vertical patterns. From the surface to 400 m, the filter is a Gustafsson filter (Gustafsson, 1996) of order 3, with a critical wavelength of 25 m. From 400 m to 1500 m, the filter is a zero-pad filter of order 2, with a critical wavelength of 100 m. From 1500 m to the bottom, the filter is a zero-pad filter or order 2, with a critical wavelength of 1000 m. To be sure that the profiles are strictly stable, they are linearly interpolated on a

250 high resolution grid of 0.5 m and then sorted.

3.3   Application on the two areas of interest

3.3.1   Stratification of the western equatorial Atlantic

The clustering method is performed on the western equatorial Atlantic profiles and the 6 clusters (named WEA-#) are sorted by the number of profiles they gather. The density profiles are measured from 1984 to 2015. The distribution of the 2421 profiles

255 into the 6 clusters is detailed in the Table 1. Note that WEA-4 and WEA-5, the two deeper pycnocline clusters, have fewer profiles than the other clusters.

     Figure 3d illustrates the median of the different typical profiles obtained for each cluster. WEA-6 contains only the density profiles that are exceptional: those 17 profiles show an offset of 1 kg.m^{-3} over the entire depth, and were measured at the same period (from October 2005 to March 2006), equally spaced by almost 10 days (Fig. 3e). These measurements have been made

---
[8]https://docs.scipy.org/doc/scipy/reference/signal.html
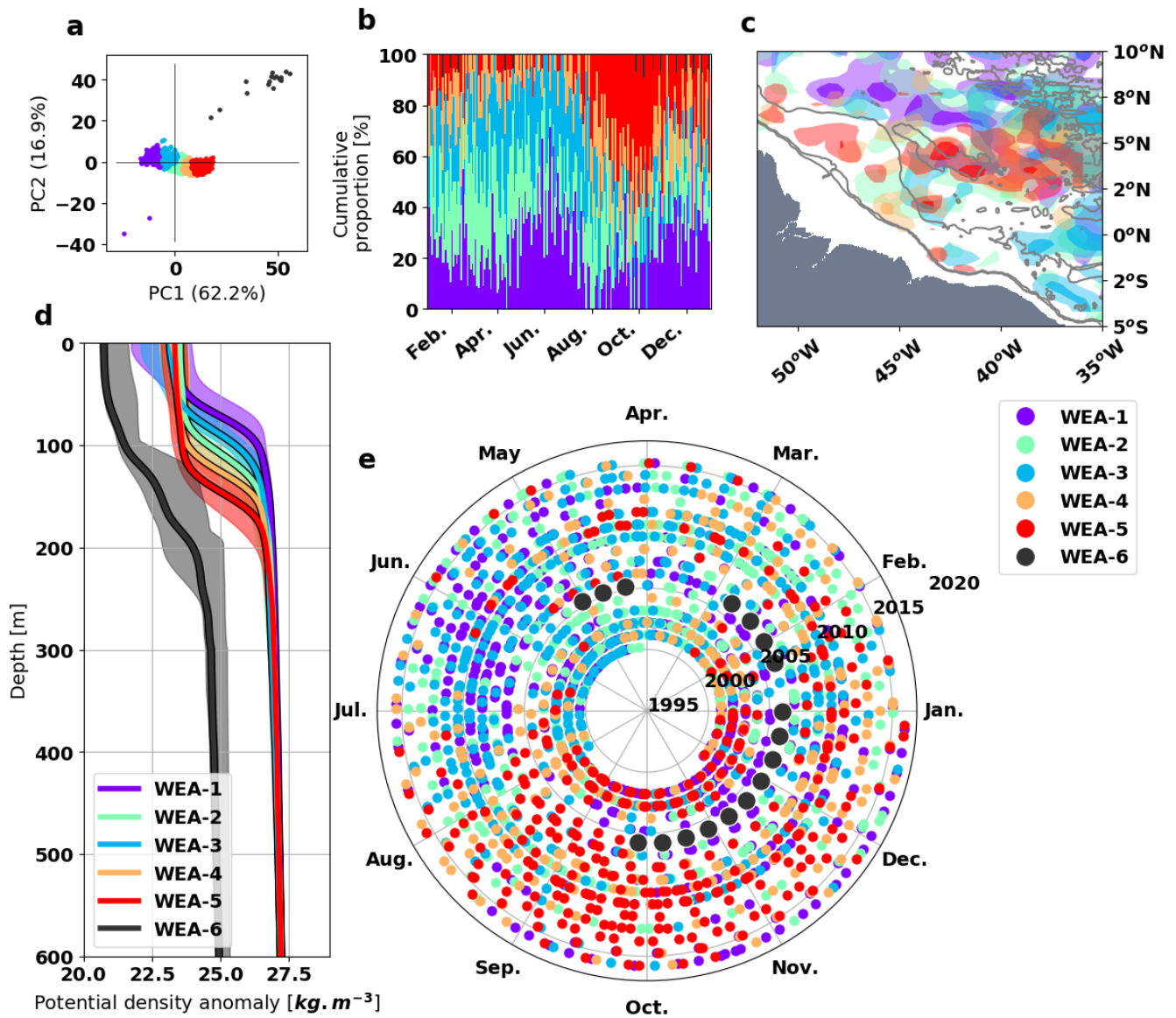
Figure 3. Classification of density profile in the western equatorial Atlantic in 6 clusters: (a) the PCA manifold of the profiles, (b) the cumulative proportion of the clusters during a mean year, (c) the spatial distribution (d) the median and the 90% interval of each cluster, (e) the measurement dates of the density profiles (the angle represent the day of the year and the distance from the center, the year of measurement). The colors of the clusters are common to all the graphs. The colored contours of (c) are set to highlight the areas gathering from 2 to 5 profiles (light color) and over 5 profiles (bold color) for each cluster. The black contours of (c) show the 200 m, 1000 m and 4000 m isobaths.

by a single ARGO float, (WMO number: 41953). This ARGO float failed its salinity measurements from the cycle 150 to 152 and from the cycle 166 to 180 (except the cycle 176) which explain the bad calculation of the associated density.

The clustering methods are efficient enough to detect those exceptional profiles that pass the standard quality control and can be used as a tool to filter them out. Gathering the suspicious profiles in WEA-6 helps to sort the data and analyse only the realistic profiles contained in the other clusters.

Figure 3d illustrates that the variability of the western equatorial Atlantic profiles is dominated by the depth of the pycnocline. This variability corresponds to the large 90% interval observed at the pycnocline depth in Figure 2a so this classification does capture the realistic variability of the density profiles. The median value of the upper surface density is centered around 1023.3 kg.m^{-3} for all the clusters. Only WEA-1 and WEA-3 show a greater variability at the surface with the 90% interval (up to 1021.3 kg.m^{-3} and 1023.8 kg.m^{-3}). All the typical profiles have a maximum stratification within the same range (Tab. 1), only the pycnocline depth differs. So, these clusters represent a good framework to investigate the influence of pycnocline depth on the ITs. From now on, the pycnocline depth will be used as a proxy to evaluate the influence of the ITs in this area.

The clusters are not strictly defined during a specific period of the year but rather during all along the year (Fig. 3b,e). In addition, the spatial distribution of the clusters is not homogeneous within the area highlighting spatially-bound ocean processes responsible for some specific stratification. As the pycnocline depth is highly controlled by the circulation, the complex spatio-temporal variability of the clusters refers to the complex spatio-temporal variability of the circulation in this region. The clusters classification enables to focus on a simple parameter (the pycnocline depth) that would be smoothed with a classical seasonal average classification.

WEA-1 is the cluster with the shallower pycnocline depth. The stronger surface stratification of the 90% interval could be due to the Amazon river plume. Indeed, the spatial distribution of WEA-1 (Fig. 3c) corresponds to the area of the Amazon river plume during the retroflection events, usually from July to December (Ffield 2005, Figure 10). This does explain the occurrence of WEA-1 from September to January but does not explain its occurrence from January to August (Fig. 3b). During this latter period the North Equatorial Counter Current (NECC, eastward) is weaker and the North Equatorial Current (NEC, westward) is a bit stronger (Richardson and Reverdin, 1987). In addition of the water masses from the Amazon plum, WEA-1 could account for the water masses of the NEC with a pycnocline around 70 m but without the surface stratification. The distribution of the seasonality of WEA-1 (Fig. B1) confirms the duality of the seasonality within this cluster: the water masses from the retroplection of the Amazon plum occur during September to February north of 5°N and the NEC water masses occur during May to July south of 5°N.

WEA-2 and WEA-3 are similar: they have the same seasonality, the same spatial coverage and gather the profiles with a pycnocline depth from 80 m (WEA-3) to 110 m (WEA-2). The North Brazil Current (NBC) is a strong geostrophic current flowing along the Amazon shelf break all year-round. The seasonality of the NBC is mainly influenced by wind-driven eddies from August to November that enhance the retroflection of the NBC water masses into the North Equatorial Counter Current (NECC, Johns et al. 1998). The seasonality of WEA-2 and WEA-3 as the large spatial distribution of the clusters clearly point out that they identify the steady state of the NBC, without the eddies.

WEA-4 and WEA-5 occur from August to November, so they have the same seasonality of the NBC eddies. These clusters gather the profiles with the deeper pycnocline. Thus they identify the profiles corresponding to the deepening of the pycnocline due to the large anticyclonic eddies of the NBC.

Garraffo et al. (2003) studied the same area looking at the different transport of water using a regional model. They separated the area in four sub-domains (Garraffo et al., 2003, Figure 11c), where two of them correspond to the area considered in the present study. They highlight that the sub-domain of WEA-2 to WEA-5 (Garraffo et al., 2003, green in Figure 11c) is influenced by the southern waters coming from the NBC. The sub-domain of WEA-1 (Garraffo et al., 2003, pink in Figure 11c) is more influenced by the NECC waters than the NBC waters. The cross-shelf transect from mooring measurements (2004, Figure 2 around 47°W) clearly shows the separation of NBC water masses, along the shelf, and the North Equatorial Counter Current (NECC) water masses off the shelf. The isopycnals' depth shows a difference of 100 m between the two waters. This difference is comparable to the difference of the pycnocline depth observed between WEA-1 around 70 m and WEA-4 and WEA-5 around 140 m. Goni and Johns (2003) used a two-layers model to convert altimetric SSH to the upper layer thickness. The authors show that the anticyclonic eddies in the NBC could increase the upper layer thickness from 20 m to 40 m (Goni and Johns, 2003, Figure 10). This difference is comparable to the difference of the pycnocline depth observed between WEA-2 and WEA-3 around 100 m and WEA-4 and WEA-5 around 140 m.

3.3.2 Stratification of the Bay of Biscay

The clustering method is also performed on the Bay of Biscay profiles. The 6 clusters are sorted by their number of profiles. The density profiles are measured from 1991 to 2015 and the separation of the 2447 profiles into the 6 clusters can be found in the Table 1. In this dataset, no suspicious profiles are detected with the clustering method, so all of the clusters will be used for the density study. Note that BB-1 has the most profiles, BB-6 has the least and the other clusters are almost equally represented.

Figure 4d shows the 6 typical profiles processed from the 6 clusters. In this area, the main variability of the profiles is dominated by the upper surface density. BB-2 and BB-6 are the only clusters to have almost the same surface density. The difference between these two clusters is the pycnocline's depth.

Figures 4b and 4e highlights that the classification corresponds to the seasonality of the profiles. Chronologically, BB-1 corresponds to winter and spring conditions with deep mixed layers with quasi-homogeneous density profiles. BB-6 corresponds to early summer with density profiles that linearly decrease up to the surface. BB-4 and BB-5 correspond to late summer and early autumn conditions with the most stratified profiles. Finally BB-2 closes the loop corresponding to late autumn with deep surface layer profiles. BB-4 and BB-5 cover the same period simultaneously and the differences are due to the intensity of the stratification: BB-4 corresponds to mild summer stratification generally in July-August and BB-5 corresponds to stronger summer stratification with more profiles in September-October.

There is also a transitional group, BB-3, composed of profiles from both before and after BB-1 (winter): in December and in May. BB-3 is designated as the shoulder season in the rest of the study. These profiles also occur during late winter corresponding to some heating events that start to build a stratification without establishing it.
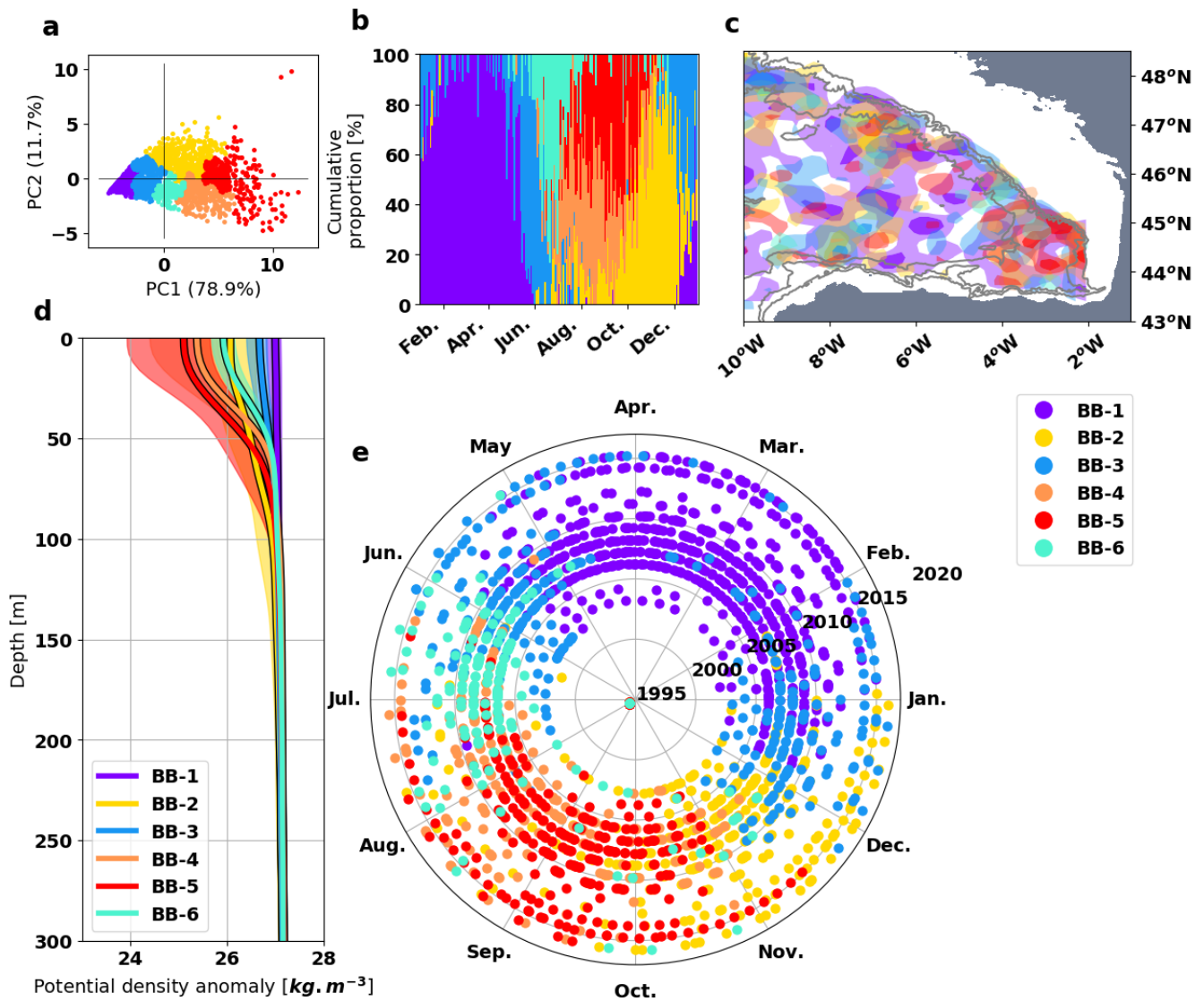
Figure 4. Classification of density profile in the Bay of Biscay shelf in 6 clusters: (a) the PCA manifold of the profiles, (b) the cumulative proportion of the clusters during a mean year, (c) the spatial distribution (d) the median and the 90% interval of each cluster, (e) the measurement dates of the density profiles (the angle represent the day of the year and the distance from the center, the year of measurement). The colors of the clusters are common to all the graphs. The colored contours of (c) are set to highlight the areas gathering from 2 to 5 profiles (light color) and over 5 profiles (bold color) for each cluster. The black contours of (c) show the 200 m, 1000 m and 4000 m isobaths.

The spatial distribution shows the cluster are almost equally distributed in the area (Fig 4c. BB-5 occurs more in the south-east of the area but it is also present elsewhere. This result confirms that the variability of the density profiles is dominated by radiative forcing rather than complex changing circulation pattern in this region.

330 As expected, the clustering methods do identify the seasonality contained in the mid-latitude variability. This classification separates the seasonal changes more distinctly than a simple three-month means: BB-1 lasts for 4 months, BB-6 lasts for 1 month, BB-4,5 last for 3 months simultaneously and BB-2 lasts for 2 months. Further comparisons are shown in the next section.

3.4 Discussions

335 The stratification of the two areas of interest are driven by very different forcing: the Amazon plume and the circulation for the western equatorial Atlantic and the radiative forcing for the Bay of Biscay. The Amazon water recirculation at the North of the domain and the NBC rings along the shelf break are limitted-extend processes whereas the radiative forcing affects the Bay of Biscay homogeneously. Thus, the spatial variability is stronger in the western equatorial Atlantic. In such area, the stratification variability presented by all the clusters does not happen in every parts of the domain but this method enables us to distinguish 340 the specificity of each sub-region at once.

In this section, some typical profiles from the clusters will be compared to seasonal climatologies (ISAS13 and BOBYCLIM) and to the three-month means made from CORA V4.3 dataset. For the western equatorial Atlantic, the two extreme clusters are chosen: WEA-1 and WEA-5. WEA-1 is compared to the spring mean because this is the season with the shallower pycnocline and because this cluster is highly represented in spring. WEA-5 is compared to the fall mean because this is the season where 345 this cluster occurs the most. For the Bay of Biscay, BB-2, BB-4 and BB-5 are used to investigate the influence of fewer months in the classification and to discriminate between mild and stronger events. BB-2 is compared to the fall mean and BB-4 and BB-5 are compared to the summer mean.

The climatology profiles are averaged on the same areas and smoothed following the method explained in section 3.2.3.

For the western equatorial Atlantic area, Figures 5a and 5b show that ISAS13 seasonal profiles are smoother than the CORA 350 V4.3 seasonal profiles. After verification, the filters applied on the profiles cannot explain such differences. ISAS13 climatology is only based on the 2004-2014 period but this different period cannot explain all the differences either. The spatial and vertical smoothing applied to construct the climatology might have been stronger in this area compared to the filtering we used here.

As expected from the climatology, the fall profiles shows a deeper pycnocline than the spring one (Fig. 5a and 5b). The climatology profiles shows a slightly smoother pycnocline than the cluster profiles. Thus, the averaging of the large diversity 355 of the profiles within one season tends to smooth the stratification and does not represent it as well as the cluster classification. WEA-1 and WEA-5 both represent a more contrasted part of the 90% interval of the seasonal profiles considered (grey patch). The shallow pycnocline cluster WEA-1 (Fig. 5a) sets the upper limit of the 90% interval of the spring climatology. The deeper pycnocline cluster WEA-5 (Fig. 5b) sets the lower limit of the 90% interval of the fall climatology. Still, the median of both clusters is part of the seasonal 90% interval, indicating that the clusters represent a right proportion of these seasonal profiles.

360 These three-month means are not highlighting the profile variability as well as the cluster classification can do. As shown above (Fig. 3c), the western equatorial Atlantic has a strong spatial variability that explains why averaging classifications are ineffective. The three-month mean is not recommended for this area that has complex circulation and mixing processes as well as a weak dependency to radiative forcing.

For the Bay of Biscay area, the BOBYCLIM and ISAS13 climatologies are almost identical for the fall and summer seasons.
365 For fall, ISAS13 profile have a small difference of $0.2 \ \text{kg.m}^{-3}$ at the surface compared to the climatology profiles made from CORA V4.3. Otherwise the CORA V4.3 seasonal mean seems representative of the Bay of Biscay climatology.

The fall climatology profiles of CORA V4.3 and BB-2 profiles are very close (Fig. 5c), the overlap of both 90% intervals is high, validating that BB-2 corresponds to the fall climatology.

The cluster classification highlighted two different clusters that correspond to the summer season: BB-4 corresponds to
370 mild summer stratification and BB-5 correspond to stronger summer stratification. Both clusters are compared to the same summer climatology. The BB-4 median profile fit exactly the summer climatology profile. The 90% interval of the BB-4 shows more stratified profiles than the summer climatology ones, especially shallower than $40 \ \text{m}$. The BB-5 profiles are indeed more stratified than the mean summer climatology profile but better fit the 90% interval of the climatology deeper than $40 \ \text{m}$ that are not represented by BB-4. The main difference between the BB-4 and BB-5 is not located at the surface but around $60 \ \text{m}$ where
375 the two 90% intervals of the clusters do not overlap each other. BB-4 and BB-5 contribute to different parts of the summer
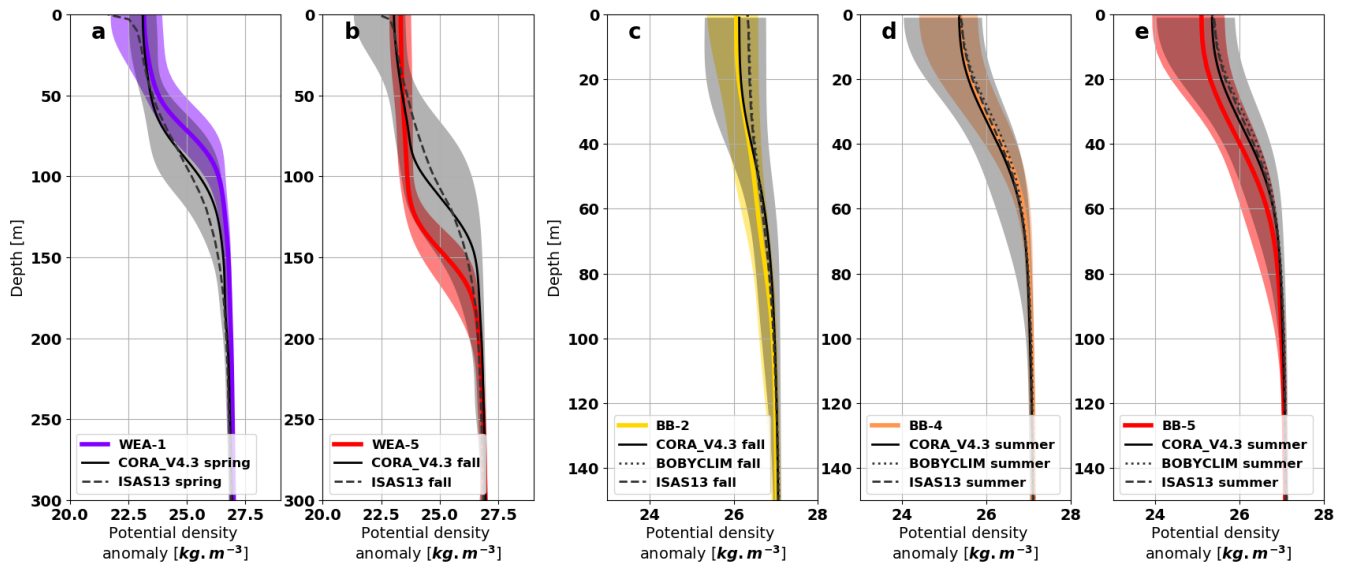
Figure 5. Climatology profiles compared to the corresponding selected typical profiles from the cluster classification: the western equatorial Atlantic (a) WEA-1 and (b) WEA-3, the Bay of Biscay (c) BB-1 (d) BB-4 and (e) BB-5. The grey shadings are the 90% interval calculated from CORA V4.3 dataset using seasonal and the colored shadings are the 90% interval of each cluster.

climatology 90% interval and enable us to separate two stratification patterns that are mixed within the classical three-month mean.

As expected, the cluster classification is more effective than the three-month mean to distinguish the different stratification regimes that can occur within a given time period. The cluster analysis enables us to describe different pycnocline states: established or transitory states and mild or extreme states. In the mid-latitude Bay of Biscay, the seasonal radiative forcing is strong and makes the stratification uniform horizontally. There, the 6 clusters classification gathers the same amount of information about the seasonality as the 12 groups of the monthly classification. Thus, the cluster classification is a more condensed approach. In the Amazon tropical regions, the spatial variability is more important due to a stronger interaction from the ocean circulation. This adds complexity to the study of the stratification variability via a time dependent classification, and requires a good knowledge of the region's circulation and water masses. As the cluster analysis does not preferably consider time dependent or space dependent classification, this method is very effective to investigate circulation-driven stratification variability, such as in the tropics.

The clustering classification is used over a long period of time in this study, but doing so does not blur the inter-annual variability. The long term variability can be observed looking at the variability within the distribution between the clusters. Figure 3e and 4e can also help to observe such variability. For example, WEA-4 and WEA-5 are usually associated with the period from August to November, but for the year 2006, WEA-4 and WEA-5 are only present from August to September. In a classical seasonal or monthly averaged classification, such long-term variability would have smoothed the stratification profiles. Here the clusters mean density profiles are based on similar instantaneous profiles, insuring more realistic profiles.

4   Sensitivity of the internal tides to the background stratification

4.1   Model configuration for the ITs simulations

The T-UGOm (Toulouse Unstructured Grid Ocean model) has been used to simulate the ITs. Initially developed to resolve the two dimensional tidal equations (Piton et al., 2020; Lyard et al., 2021), this model has been extended to resolve the three dimensional tidal equations in the frequency domain (Nugroho, 2017; Lyard *et al., in prep.*). The model configuration is set to be hydrostatic and with a free surface. The 3D version uses Lagrangian layers that follow the fluid displacement in the vertical dimension. The experiments are focused on the M2 major tidal component in the two areas of interest and are based on the stratifications described in the previous section. The frequency domain calculation uses the tidal dynamical equations expressed in the complex, frequency space. This allows for much faster computation time than the time-stepping calculation but does not support a stratification evolution over time and the simulated ocean needs to be at rest. These concerns affects the density profile structure that the model can handle. If the density profile is unstable, high amplitude instabilities are created because the stratification induces vertical motions rather than acting as a restoring force.

All simulations are carried out with the same configuration and the same inputs that are shown in the Table 2. The reference latitude θ_{ref} for the calculation of the Coriolis parameter is set differently for each area: $\theta_{ref} = 0°N$ for the western equatorial Atlantic and $\theta_{ref} = 47°N$ for the Bay of Biscay. This enables us to compare the simulations with ITs measurements and realistic

Table 2. Inputs of COMODO-revised simulations

Name	Variable	Value
Horizontal diffusion	k_H	1.10^{-3} m^2.s^{-1}
Vertical diffusion	k_z	1.10^{-3} m^2.s^{-1}
Roughness length	z_0	3.10^{-3} m
Barotropic tidal velocity	u	10 cm.s^{-1}
	v	0 cm.s^{-1}
Relaxation length	L	42.5 km
Relaxation time scale	τ	72 min

simulations. A single density profile is used to set the stratification uniformly over all of the domain. The typical density profiles

410 from the above classifications (sections 3.3.1 and 3.3.2) are used and one simulation is made for each profile. As explain earlier, the density profile needs to be strictly stable because the frequency domain calculation does not allow the density to adjust as in a time stepping calculation.

This model is applied using the academic configuration from COMODO project (Ocean Modeling Community, 2011-2016, PI: L. Debreu, Soufflet et al., 2016) for the study of the internal waves generated on a continental slope (Nugroho, 2017). The

415 project was originally built to compare different ocean models and T-UGOm 3D was one of them. The original configuration is based on the configuration of Pichon and Maze (1990): a flat bottom ocean of 4000 m depth in the abyss (on the left) and 200 m depth on the shelf (on the right); the domain is wide of 880 km along the axis x and large of one horizontal mesh, equal to 1 km. The slope is described by the equations:

$$\begin{cases} \frac{d^2b}{dx^2} = -0.5\left(1 - \frac{cos(\pi(x-x_0))}{x_1-x_0}\right) & \text{for } x_0 < x < x_1 \\ \frac{d^2b}{dx^2} = -1 + 0.5\left(1 + \frac{x_2-x_1}{x_3-x_1}\right)\left(1 + \frac{cos(\pi(x-x_2))}{x_2-x_1}\right) & \text{for } x_1 < x < x_2 \\ \frac{d^2b}{dx^2} = 0.5\frac{x_2-x_0}{x_3-x_1}\left(1 + \frac{cos(\pi(x-x_2))}{x_3-x_2}\right) & \text{for } x_1 < x < x_2 \end{cases} \qquad (4)$$

420 where b is the bathymetry, $x_0 = 426$ km, $x_1 = 443$ km, $x_2 = 479$ km and $x_3 = 484$ km. This bathymetry is similar to an averaged continental slope, the comparison to realistic bathymerty of the two areas of interest is shown on Figure C1. The domain is described by 1760 Finite Element triangles using LGP1xLGP0 convention. LGP1 refers to the summit of the triangles where the pressure and elevation are set continuously from one triangle to another (Lagrange Finite Element of 1 degree of freedom). LGP0 refers to the barycenter of the triangle where the velocity is set (Lagrange Finite Element of 0 degree of

425 freedom). On the vertical dimension, density is piecewise linear (*i.e.* linear inside layers with possible discontinuities at layers' interfaces), and velocity is uniform. The model is based on the primitive momentum equations, continuity equation and density advection equation. The model unknowns are the level displacements (including the free surface), horizontal velocities and density anomalies (due to advection in layers). However, a 3D wave-equation approach allows us to form a linear system where unknowns are limited to level displacements and density anomalies, velocities being then deduced once the 3D wave-

430 equation system is solved.

This configuration places the slope in the center of the domain but this is not the optimal configuration for the present ITs study. As explained in the introduction, the wave beam slope is controlled by the stratification until it reaches the bottom. So the depth also controls the wavelength of ITW. This configuration only allows us to resolve around 2 or 3 times the wavelength in the abyss domain whereas more than 20 or 30 times the wavelength is resolved in the shelf domain. To compensate for this

435   difference, the slope is shifted toward the shelf by 220km. This allows us to resolve around 4 or 5 times the wavelength in both domains.

After taking care of the horizontal resolution of the ITs, the vertical resolution needs to be investigated too. As shown in the previous section, the density profiles are steeper at the surface than at the bottom of the ocean. This means that the dynamics of the ITs are more different from one layer to another near the surface than at the bottom. Hence, a finer resolution at the surface

440   is needed in order to resolve those dynamics. The vertical distribution of the 80 σ-layers (which follows the bathymetry) is set following a surface cosine: the layer thickness is thinner at the surface and larger at the bottom, the decrease is set by a cosine between 0 and $\pi/2$. Using σ-layers helps to get a strong resolution in the generation area, at the top of the shelf.

The Karman-Prandtl equation is used to calculate the bottom velocity affected by the bottom friction, as described for the AMANDES tidal model in the Amazon estuary (Le Bars et al., 2010). Using a frequency domain calculation, there is no

445   time-step to set the bottom friction. So, an iterative process is used in order to make the bottom velocity converge, solving the equations 4 times, each time using the previous bottom velocity. The model uses logarithmic buffer areas at the open boundaries (both sides) in order to stabilize the results. The relaxation term R is expressed as follows:

$$R = \frac{exp\left(-\frac{d}{L}\right)}{\tau} \tag{5}$$

with $\tau = 72$ min being the relaxation time scale, d the distance from the boundary and L the relaxation length. In order to

450   prevent the energy being reflected at the boundary, the relaxation length is extended from 20.0 km to 42.5 km on both sides.

In order to separate properly the baroclinic tides (ITs) from the barotropic tides, the solution is decomposed into vertical modes following the methods described in Nugroho (2017). For the following discussion, mode 1 and higher will refer to vertical baroclinic modes whereas mode 0 will refer to the vertical barotropic mode.

4.2   Modeling results on the two areas of interest

4.2.1   Impacts of the western equatorial Atlantic stratifications

455

As explained in section 3.3.1, the typical profiles from the Amazon clusters have almost the same stratification maximum and only the pycnocline depth differs in this area. From now on, these clusters profiles will be sorted by the depth of the pycnocline: WEA-72 m, 88 m, 108 m, 128 m, 148 m (corresponding to WEA-1, 3, 2, 4, 5; Tab. 1).

Before detailing the impacts of pycnocline depth on the surface elevation, its influence on the baroclinic vertical modes is

460   first investigated. Figure 6 (left panels) illustrates the three first baroclinic modes for all of the typical density profiles. The depth of the extremum of all modes is influenced by the pycnocline depth (the black dots on the plots).
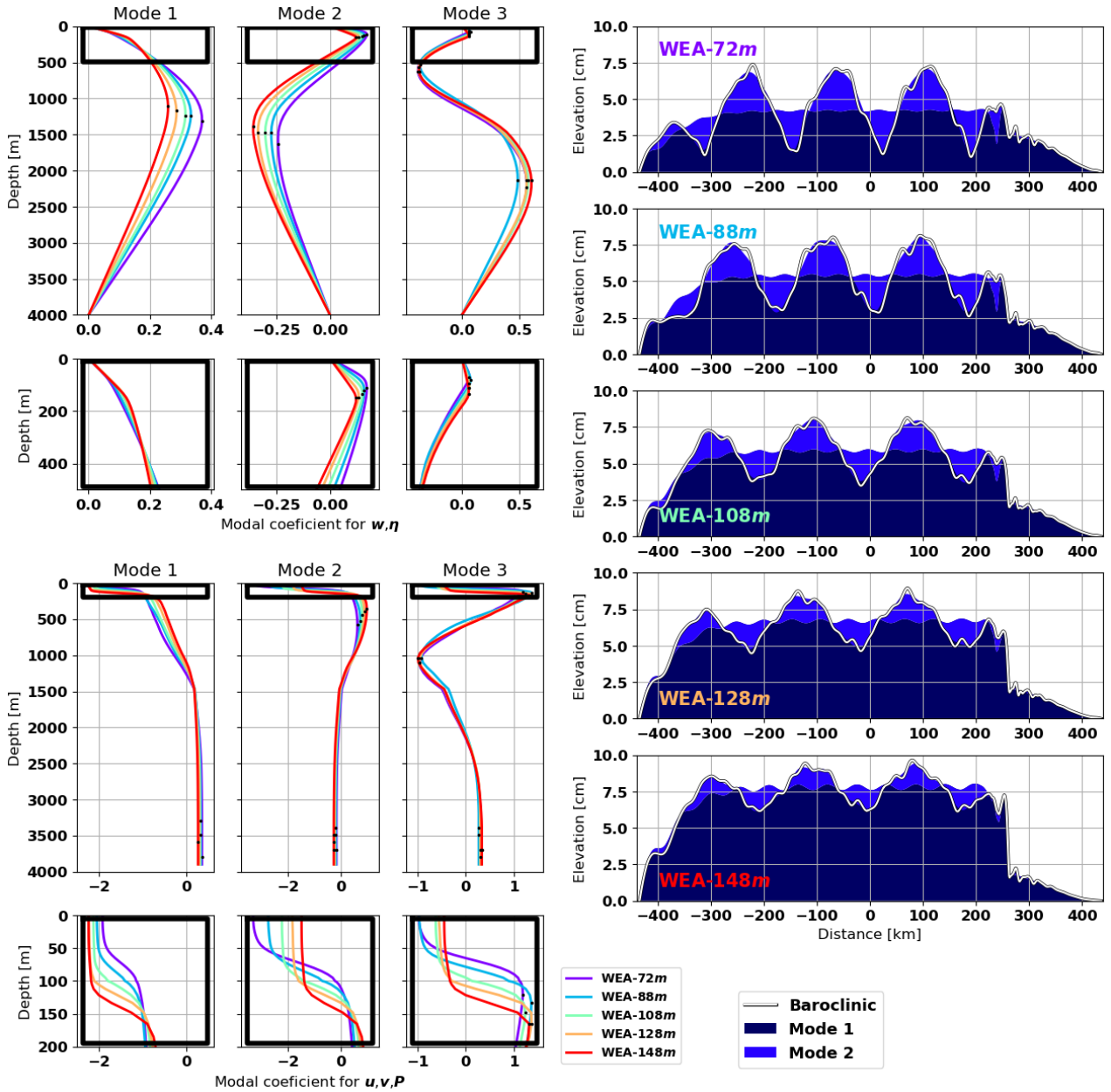
Figure 6. Baroclinic modal structures for the three first modes (left panels) and simulated amplitude of baroclinic surface elevation for the five first modes (right panel) for all the typical density profiles of the western equatorial Atlantic. The modal structures are different for vertical processes (w and η, upper left panels) and horizontal ones (u,v and P, lower left panels). The black points show the extremums of the modes. The simulations are sorted with respect to the depth of the pycnocline. On the right panels, the white line represents the sum of the baroclinic modes, the colored patches represent the modal contribution to the complex sum: if the patch of mode n is located on top of the sum line, then mode n works against mode $n-1$.
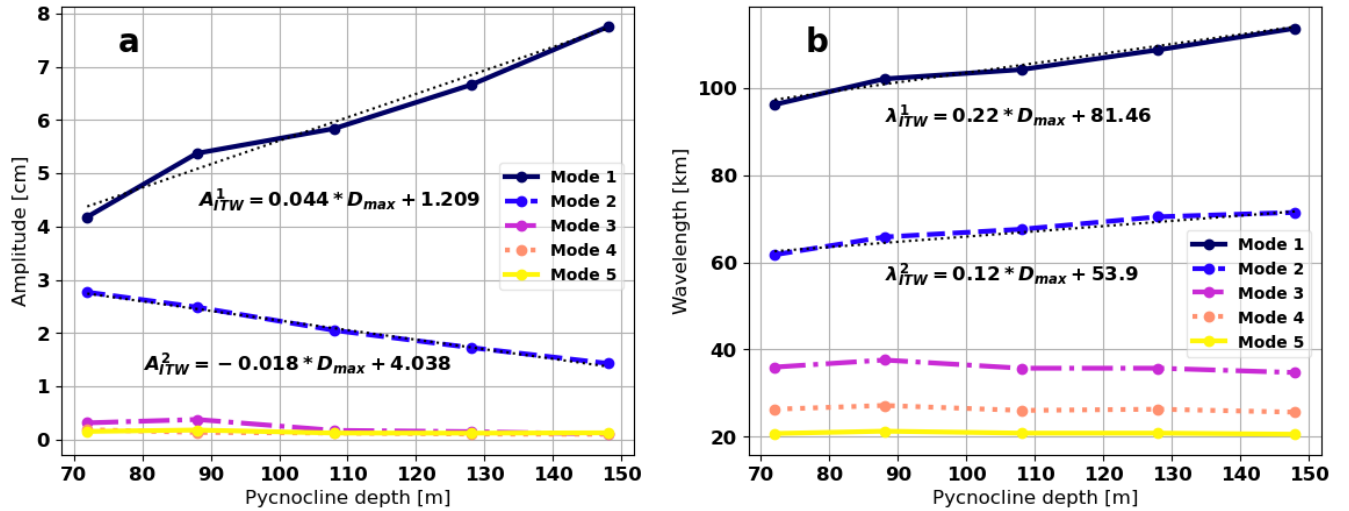
Figure 7. (a) Amplitude and (b) wavelength of the surface elevation for each vertical mode with respect to the pycnocline depth. The calculations are based on the western equatorial Atlantic simulations over the abyssal domain (-300 km$< x < 200$ km). The fit equations for the two first modes are shown below the curves (with A_{ITW}^n the ITs' surface amplitude for mode n, λ_{ITW}^n the ITs' surface wavelength for mode n and D_{max} the pycnocline depth).

First, concerning the modes of the vertical structures w and η. For mode 1, the deeper the pycnocline, the further the mode is shifted toward the surface. For mode 2, the deeper the pycnocline, the further the mode is shifted toward intermediate layers: the first extremum is deeper and the second one is shallower. For mode 3, the pycnocline depth only affects the first extremum: with a deeper pycnocline, the extremum is deeper. The same observation can be made for the modes of horizontal structures u, v and P. At the surface, while for a deeper the pycnocline, mode 1 is stronger and the higher modes are weaker. The impact of the pycnocline depth on the mode shifts seems linear for mode 1 and 2.

The only exception to this pattern happens for the horizontal structure of mode 3 at the surface: WEA-70 m and WEA-85 m have the same amplitude, whereas WEA-85 m was expected weaker. This difference can be due to small density differences at the surface between the typical density profiles of about 0.02 kg.m^{-3} which is the smallest difference at the surface between the clusters.

Figure 6 (right panels) illustrates the simulated amplitude of the baroclinic surface elevation. For the western equatorial Atlantic simulations, the overall amplitude of the baroclinic elevation scales from 7 cm to 10 cm with no contribution of the modes higher than 2. When the pycnocline deepens, the total amplitude of the elevation increases with a dominance of mode 1 over mode 2. The number of troughs for mode 2 decreases with a deeper pycnocline. The wavelength for the combination of all modes seems to be larger with a deeper pycnocline.

To investigate this impact, the wavelength of each mode has been calculated for the abyssal domain (from -300 km to 200 km). The wavelength is calculated following the method of Welch (1967) with 200 elements per segment and a zero

padding of 5000 elements. Using the zero padding enables to increase the resolution of larger wavelengths but creates irrelevant
wavelengths, so all the wavelengths larger than 500 km are cleared ($\lambda_{\max} = Ndx$).

Figure 7 presents the evolution of the ITs amplitudes and wavelengths at the surface with respect to the pycnocline depth.
As expected with the shape of the modal structures, modes 1 and 2 are linearly controlled by the pycnocline depth. A deep
pycnocline increases the wavelength of mode 1 and 2 of the surface elevation with a slightly stronger impact on mode 1.
The amplitudes and wavelengths of modes 3, 4 and 5 seem to slightly decrease with the increasing depth of the pycnocline.
Empirical relations for modes 1 and 2 can be found by fitting the curves.

These relations could be a useful proxy to determine the ITs' surface wavelengths but have to be used with extreme caution.
As explained in the introduction, the ITs' surface wavelength is directly dependent on the bathymetry. In this simulation the
bathymetry is always the same, allowing us to formulate this empirical relation. Hence, this relation is only valid in the 4000 m
deep tropical areas studied here. Other tests should be made in order to integrate depth variations into these empirical relations.

This variation of the ITs' surface wavelength can lead to a strong aliasing of the ITs corrections and altimetric observations
if this variability is not taken into account. For example, the wavelength difference for mode 2 between WEA-71 m and WEA-
148 m is about 10 km. With only three occurrences of the wave beam at the surface, the shift associated to mode 2 is about 30
km. The correction that only use a wavelength of 60 km to corrected mode 2 (corresponding to WEA-71 m), will be in phase
opposition after only three occurrences if the stratification leads to an actual wavelength of 70 km (corresponding to WEA-148
m). This rough calculation helps to understand why small changes in the wavelength can completely change the shape of the
surface ITs signature.

Tchilibou et al. (2019) reported a similar observation comparing two simulations from El Niño and La Niña context in the
Salomon Sea. In this region, the El Niño stratification is characterized by a shallow pycnocline and the La Niña stratification
is characterized by a deep pycnocline. The authors pointed out that this stratification variability is one of the sources of the
non-stationarity of the ITs observed using altimetric SSH. The surface elevation of the model outputs seems to present a larger
wave beam during La Niña than during El Niño (Tchilibou et al., 2019, Figure 8). In the western equatorial Atlantic area, the
high dependency of the wavelength to the pycnocline depth could be a major contribution to non-stationary ITs that appear in
the study of Zaron and Ray (2017).

This result reinforces the importance, in the future, to properly take into account the pycnocline depth regimes in order to
estimate a more accurate ITs' surface signature. The pycnocline depth could be used as a proxy to estimate the wavelength of
ITs and then, better constrain the ITs atlases. The simulations of the different clusters should be done for a broad range of max-
imum bathymetry. This work could enhance the empirical relations of ITs amplitude and wavelength adding the dependency
to the bathymetry.

To compare the T-UGOm simulations to realistic studies, some atlases of ITs and a realistic NEMO simulation are used. In
Ray and Zaron (2016), the ITs' surface elevation amplitude is on the order of 6 cm. In Zaron (2019), the ITs' surface elevation
amplitude is on the order of 4 cm. This difference can be first explained because long term altimetry harmonic analysis only
extracts the stationary part of the ITs (as explained in the introduction). So these empirical atlases only resolve the mean
stratification context of the ITs. During the 2015 NEMO model simulation of Ruault et al. (2020), the ITs' surface elevation

amplitude is on the order of 5 cm (publication in preparation). With an amplitude ranging between 7 cm and 10 cm, the simulated amplitudes are higher compared to those altimetry-derived atlases and realistic simulation but have the right order of magnitude.

In Table 1, WEA-1, WEA-2 and WEA-3 (WEA-72 m, WEA-108 m and WEA-88 m) represent more than 70% of the density profiles. These clusters only represent profiles with a shallower pycnocline. WEA-108 m is the closest cluster to the median of all the profiles, this cluster is used for the comparison with realistic products. The ITs' surface elevation amplitude of WEA-108 m is 7.5 cm, closer to the altimetry atlases than the 10 cm of WEA-148 m. However, the intensity of the ITs are also strongly influenced by the intensity of the barotropic tidal energy flux directed off the shelf slope. The barotropic currents are mostly set through the barotropic boundary conditions (see Tab. 2 for the barotropic currents used in the present study). To some extent, only the relative changes of ITs characteristics should be considered quantitatively when comparing our academic experiments to empirical analysis or 3D realistic simulations.

4.2.2 Impacts of the Bay of Biscay stratifications

In this section, the clusters are sorted following the period of the year they represent: BB-1,3,6,4,5,2 To facilitate the description, the clusters are renamed with the corresponding season: BB-winter, shoulder, spring, summer, hot-event, fall.

In the Bay of Biscay case, the differences between the typical profiles are not driven by the surface pycnocline depth but by the stratification value in the upper surface layer (<25 m, Fig.4b). Indeed, the maximum value of N has a great variability whereas the pycnocline depth is always close to 40 m (Tab. 1) except in winter where there is no surface stratification (BB-1 in the table). Because of the variability in N, the interpretation of the stratification impact on the baroclinic modes (Fig. 8 left panels) is more complex than for the western equatorial Atlantic simulations.

The easiest way is to proceed from lower modes to higher modes. Mode 1 is almost the same for all the clusters for both vertical (w and η) and horizontal structures (u,v and P). So mode 1 is not sensitive to the variability of the stratification. Indeed, mode 1 is built upon the constant maximum at 800 m (Fig. 2f).

Mode 2 presents the same pattern for both vertical and horizontal structures: the more stratified the cluster is, the further the mode is shifted toward the surface. The clusters are sorted as follows: BB-shoulder, BB-spring, BB-fall, BB-summer, BB-hot-event. BB-winter is excluded from this pattern . For mode 2 horizontal structures (u, v and p), BB-winter and BB-shoulder are exactly the same at the surface and BB-winter is stronger at intermediate layers. This can be due to the fact that the only stratification of the BB-winter profile is located around 800 m. For mode 2 vertical structures (w and η), BB-winter is stronger than BB-shoulder at the surface. No explanation could be found for this pattern.

For mode 3 vertical structures, the pattern at the surface is the opposite of mode 2: BB-hot-event, BB-summer, BB-fall, BB-spring. BB-winter and BB-shoulder are excluded because they are weaker than BB-hot-event. For intermediate layers BB-shoulder fits to the pattern . For mode 3 horizontal layers at the surface, the previous pattern is completely irrelevant. The clusters are classified as follows: BB-winter, BB-shoulder, BB-hot-event, BB-fall, BB-summer, BB-spring. This could be due to the stratification at the surface, as the density profiles seem very straight at the surface in Figure 4d.
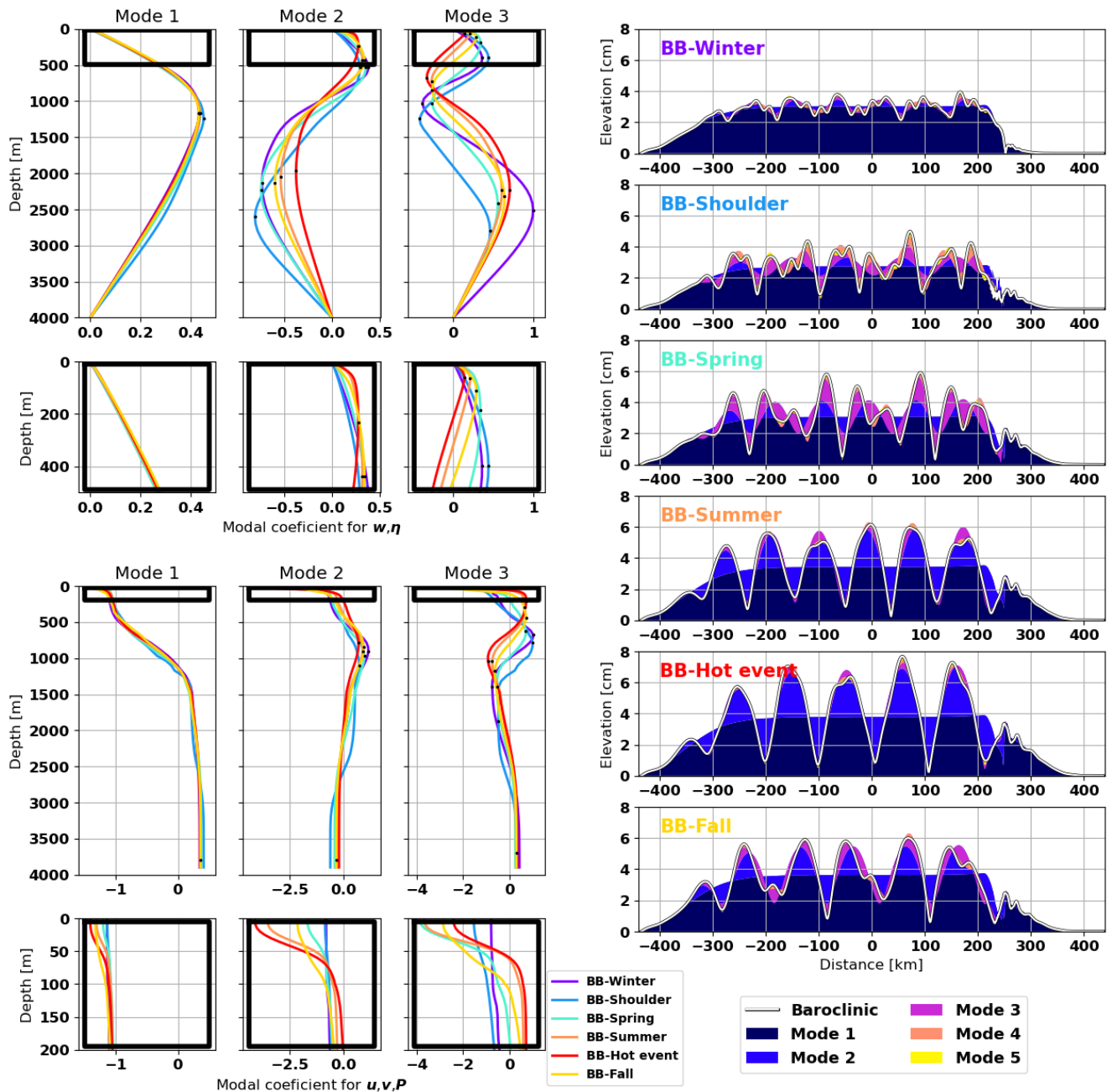
Figure 8. Baroclinic modal structures for the three first modes (left panels) and simulated amplitude of baroclinic surface elevation for the five first modes (right panel) for all the typical density profiles of the Bay of Biscay. The modal structures are different for vertical processes (w and η, upper left panels) and horizontal ones (u,v and P, lower left panels). The black points show the extremums of the modes. The simulations are sorted with respect to the seasons. On the right panels, the white line represents the sum of the baroclinic modes, the colored patches represent the modal contribution to the complex sum: if the patch of mode n is located on top of the sum line, then mode n works against mode $n-1$.

The overall baroclinic amplitude of the surface elevation ranges between 3 cm and 8 cm (Fig. 8 right panels). Modes 1 and 2 are stronger with the increase in stratification between 20 m and 60 m: being 3 cm-0.5 cm for BB-winter and 3.8cm-3 cm in the highly stratified BB-hot-event. Mode 2 is more sensitive to the stratification: it is almost equivalent to mode 1 for BB-hot-event whereas it is almost null for BB-winter. Mode 3 is stronger dunring BB-shoulder, BB-spring and BB-fall than for other stratification where it is almost null. This confirms the observations made for the modal structures. Modes 4 and 5 are only visible during BB-shoulder. These results also highlight the fact that ITs are completely absent from the shelf domain ($x > 250$ km) during BB-winter, when the stratification between the surface and 200 m is null and does not support the propagation of ITs.

In summary, in the Bay of Biscay, mode 1 is controlled by the maximum of N at 800 m, mode 2 is controlled by the value of N between 20 m and 40 m and mode 3 might be controlled by the value of N between the surface and 20 m.

The T-UGOm simulations are also compared to the same atlases as for the western equatorial Atlantic. In Ray and Zaron (2016), the ITs' surface elevation amplitude is around 1 cm. In Zaron (2019), the ITs' surface elevation amplitude is around 2 cm. The simulated amplitudes between 3 cm and 8 cm are higher compared to those altimetric atlases and simulation but are the right order of magnitude. The difference could come from the difference in the barotropic tidal forcing and the bathymetric slope that are arbitrary set in these idealized simulations. But as explained in the introduction, the empirical models of ITs also probably under-estimate the amplitude of the ITs' SSH because of the large non-stationary component in this region. Also, the altimetric observations are not suitable to capture the surface signature of the higher vertical modes because their wavelengths are too small compared to the spatial distribution of the observations. So the results of Ray and Zaron (2016); Zaron (2019) mostly highlight the relative stationarity of the first mode, and might not include the weaker ITs amplitudes from the higher modes.

The number of peaks of mode 2 occuring in the domain from -300 km to 200 km gives an approximation on the wavelength sensitivity in the Bay of Biscay: there are 6 peaks of mode 2 for BB-winter, 5 for BB-shoulder, 6 for BB-spring, 6 for BB-summer, 5 for BB-hot-events and 5 for BB-fall. The difference is clearly visible between BB-summer and BB-hot-event at -50 km: the surface amplitude combination of the modes is minimum for BB-summer and maximum for BB-hot-event. This suggests that the stratification contributes to the variability of the wavelengths of the ITs modes in the Bay of Biscay as well.

As previously explained, the surface pycnocline depth is not the right parameter representing the ITs variability in this area. The values of the stratification at different depths have been explored but the wavelengths are not influenced in the same way as the amplitudes are. As no adequate proxy has been actually found (such as the pycnocline depth for the western equatorial Atlantic), both the ITs' surface amplitudes and wavelengths are processed seasonally. A climatology has been constructed with a time step of 3 days. For each period of 3 days, the amplitudes and wavelengths of each mode are calculated from the weighted mean of the clusters distribution in the dataset. The weighted standard deviation is also calculated to evaluate the variability inside each time step.

Figure 9 shows this climatology. As expected, the amplitudes and the wavelengths do not present the same pattern. To simplify the descriptions, BB-winter characteristics are used as a reference for the comparisons. The amplitudes of the modes are very contrasted through the year. Mode 1 is stronger from August to October with a homogeneous value of 3.5 cm through
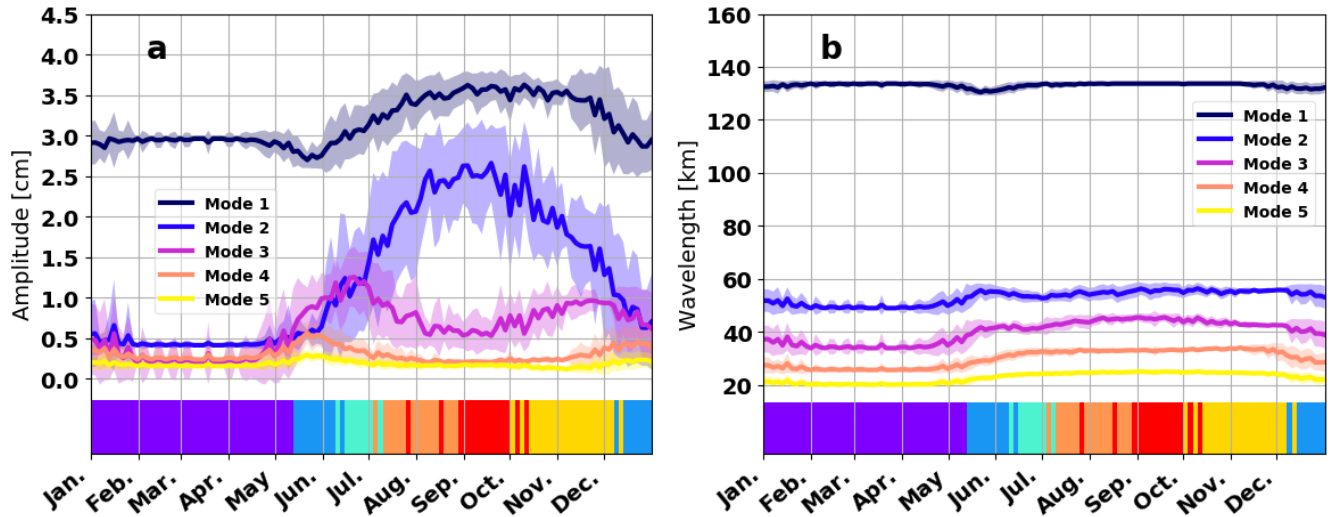
Figure 9. Weighted mean of (a) the amplitude and (b) the wavelength of the surface elevation for each vertical mode during the year. The calculations are based on the Bay of Biscay simulations over the abyssal domain (-300 km$< x < 200$ km). The climatology is built with a time step of 3 days where the ratio of each cluster is used as the weight. The shading represents the weighted standard deviation. The ruler at the bottom of the plots shows the color of the dominant cluster along the year.

this period. It became weaker in May (around 2.7 cm), and maintains a plateau of 3 cm from December to May. Mode 2 has larger amplitude variability compared to other modes. From 0.5 cm in winter and spring, it increases to 2.5 cm in September, then decreases until January. Even with smaller amplitude, mode 3 has significant amplitude variability: two peaks at 1.3 cm

585   and 1.0 cm happen in June and November, otherwise stabilized around 0.3 cm. This particular pattern seams to be due to the stratification near the surface, stronger in BB-shoulder and BB-spring compared to other cluster that are well mixed near the surface. Modes 4 and 5 amplitudes patterns are close to mode 3 one but the peaks happen in May and December, so mainly caused by BB-shoulder surface stratification.

The wavelengths have a weak variability between all the simulations. This explains why the standard deviation is almost

590   null. The wavelength of mode 1 is almost constant during the year, it only decreases in May and December, due to BB-shoulder stratification. The wavelength of modes 2, 3,4 and 5 have similar pattern around two values: lower from February to May (50 km, 35 km, 26 km and 20 km) and stronger from June to December (56 km, 45 km, 33 km and 25 km). The shifts are stronger for modes 3 and 4 and is clearly due to the presence of surface stratification after winter. In Figure 8, the closest extremum to the surface of the modal structure of horizontal structure (u, v, P) is affected by the stratification and is not located at the same

595   depth. For mode 2, the variability of the depth is around 400 m but for mode 3, the variability is around 1200 m. This could explain why the wavelength of mode 3 is more affected than the wavelength of mode 2. Thus, the vertical modal structure and their variability based on the stratification can give a good estimation of the wavelength response.

As with the western equatorial Atlantic, these variations in wavelength can be responsible for significant shifts in the surface elevation patterns and lead to wrong corrections of the ITs' surface signatures. Still, the relatively weak variability in wavelengths might explain why the non-stationarity of the ITs is weak in this area in the maps of Zaron and Ray (2017). This cluster-based climatology is the first step to build an evolving correction of the ITs during the year. This climatology could help to better estimate the amplitude observed from altimetric observations.

4.3 Discussions

The ITs simulation experiments clearly highlight the dependency of the ITs patterns of amplitude and wavelengths (hence surface signature) on the stratification. They provide a quantitative estimate of the ITs temporal variability due to the ocean background stratification changes only. This background stratification is a key process for the ITs generation and one of the processes that control the ITs propagation.

As the focus of this study was the background stratification, other parameters have been set equally in both configurations (western equatorial Atlantic and Bay of Biscay). The slope and the barotropic tidal forcing are two key parameters for the ITs generation. These parameters, combined with the background stratification, directly control the ITs generation and with it the amplitude of the surface elevation. This is why the present study is focused on the inter-comparison of background stratifications rather than the realistic values of ITs. This enables us to compare the different stratification pattern between the two areas of interest and conclude that the pycnocline depth (western equatorial Atlantic) leads to a stronger impact over ITs surface signature than the surface stratification (Bay of Biscay)

The slope of the shelf break is a bit steeper for the Bay of Biscay one than for the amazonian one. Based on FES-2014b (Lyard et al., 2021), the M2 tidal barotropic currents in front of the western equatorial Atlantic are around 3 $\mathrm{cm.s}^{-1}$ and in front of the shelf of the Bay of Biscay are around 5 $\mathrm{cm.s}^{-1}$. The forcing used for the COMODO test case was 10 $\mathrm{cm.s}^{-1}$ which is much stronger than the realistic forcing. This could explain why the simulated amplitude are stronger than the one of the atlases in both cases. Using the realistic slope and tidal forcing could also reduce the difference of amplitude between the two areas. Indeed, the tidal forcing is stronger in the Bay of Biscay but the background stratification is stronger in the western equatorial Atlantic.

To further explore the comparison with realistic products, the ITs' stationary surface wavelength is also extracted from the atlas HRET V8.1 (Zaron, 2019) and from the NEMO simulation (Ruault et al., 2020). The comparison is only made for the western equatorial Atlantic. The wavelength calculation is made with a 2D Fast Fourier Transform of the ITs' surface elevation complex field. Using the complex field enables us to extract the direction of propagation in addition to the wavelengths. Because the NEMO simulation only is for the area 2°S-9°N, 52°W-43°W, the same area is used for HRET.

Figure 10 first shows that the wavelength pattern is very similar between HRET and NEMO. They highlight a major wavelength of 110-120 km propagating northeastward and secondary wavelengths from 70-80 km propagating in the same direction. In NEMO, the propagation of this secondary wavelength is stronger and wider than in HRET. This could be due to the constraints used in HRET to better structure the ITs. The phase field of HRET shows ITs propagation with wave crests roughly linear whereas the NEMO phase field shows them more smoothly curved (Fig.10c,d).
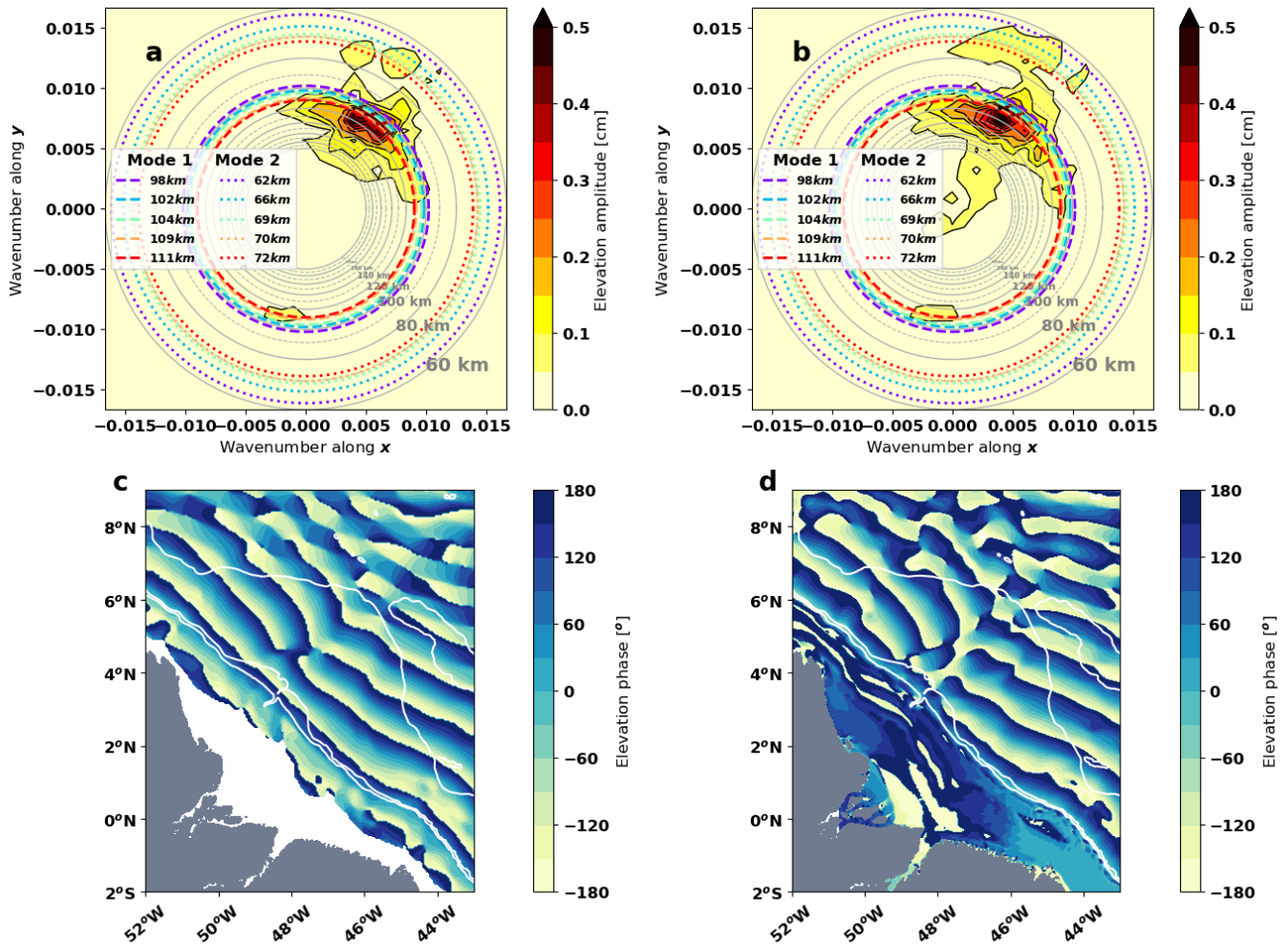
Figure 10. Two dimensional Fast Fourier Transform of the baroclinic surface elevation for M2 from (a) HRET V8.1 atlas (Zaron, 2019) and (b) a realistic regional NEMO simulation for 2015 (Ruault et al., 2020) and (c,d) their associated phase field. The grey rings represent the wavelength grid scale and the colored rings represent the wavelengths of modes 1 and 2 for the T-UGOm simulations. The value of the wavelengths is shown in the legend.

The wavelengths in HRET and NEMO are coherent with both modes 1 and 2 wavelengths calculated from the clusters, but models' wavelengths are slightly longer than the averaged cluster wavelengths. As explained in the introduction, the ITs' surface wavelength is directly dependent (roughly linearly) on the bathymetry. The bathymetry of the T-UGOm simulations is set capped to 4000 m whereas the real bathymetry in the area can extend down to 4500 m next to the continental slope and down to 5000 m further north. These bathymetry differences likely explain almost all of the wavelengths differences. Still, the stratification variability could also contribute to these differences. The ITs' surface wavelength of WEA-148 m is around 115 km for mode 1 and 70 km for mode 2. This fit the wavelengths of HRET and NEMO almost perfectly.

More realistic experiments with various uniform stratifications in a realistic regional grid are presently carried out for the ITs in the Bay of Biscay with the model SYMPHONY (Marsaleix et al., 2008). So far, these simulations lead to similar conclusions compared to the ones obtained with the T-UGOm academic configuration (Barbot, 2021, PhD thesis, in preparation). This confirms that the T-UGOm simulations, although very academic, are in the right range compared to more realistic cases. Such idealized simulations are thus a good way to estimate the ITs properties before running more realistic but complex 3D simulations.

The idealised approach could also help to furnish a simple correction from the background stratification in order to better understand the complex dynamical interactions between the ITs and the mesoscale oceanic circulation. This correction could be enhanced using the clustering methods with these a priori cluster to link the density profiles to the closest cluster. Once the density field is classified, the corrections from the corresponding idealised case could be applied.

5 Conclusions

The classification of density profiles through clustering methods is very useful to describe both spatial and temporal variability of the stratification. As shown, this methodology can highlight different regimes of stratification that are linked to seasonality (Bay of Biscay) or to spatial distribution (western equatorial Atlantic) at the same time. Thus, any kind of stratification variability can be handled with a single methodology. Especially for cases that are not driven by seasonality or for cases with clear spatial distribution variability, this methodology is a great improvement compared to mean state and seasonal classification.

The users of such a cluster methodology need to be aware of some specific parameters. The first and more important one is the normalization of the profiles. This choice is important and can change the goal of the classification. The second point is the choice of the clustering method for systematic or automated stratification studies. Many of clustering methods exist with different performances, but a first selection can be made by looking at the distribution of the PCA manifold.

For the western equatorial Atlantic, the clusters help to highlight the strong spatial variability of the stratification, and the dominance of the pycnocline depth in this variability. In the Bay of Biscay, the cluster does reproduce the seasonality of the stratification and highlights two different regimes for the summer.

The present results of ITs simulations allow a better understanding of the ITs dependency on the background stratification. This dependency not only occurs in areas driven by the radiative forcing but also in areas driven by the circulation. First, the stratification variability has a stronger impact on ITs if the stratification is composed of only one pycnocline. In the tropics,

such a pycnocline is maintained year-round and is stronger than the ones at mid-latitudes. Second, the pycnocline depth has stronger impacts on both amplitudes and wavelengths of the two first modes of the ITs than the surface stratification. In the presence of a strong ocean circulation, the variability of the pycnocline depth is more important. Third, the surface stratification variability, driven by the radiative forcing has a stronger impact on the amplitudes of modes 2 and 3.

The high dependency of the ITs horizontal wavelengths, amplitudes and modal distribution to the stratification regimes is a major result of this study and also leads to a better understanding of non-stationarity of the ITs. This result will impact on the future works dedicated to ITs' surface elevation observation and prediction. Temporal harmonic analysis of the surface elevation can only estimate the ITs anomalies of the stationary part, dominated by mode 1. The present study highlights that mode 2 can be nearly as strong as mode 1 in both areas of interest. This result suggests that time harmonic analysis underestimates the ITs multi-mode amplitude and omits the ITs wavelength of mode 2. Moreover, the ITs' surface elevation corrections based on such methods, without realistic horizontal wavelengths, could create a fictitious signal in the corrected observations from the aliasing between the real ITs wavelengths and the wavelength of the correction. The frequency domain modeling proposed in this study could be used to build multiple simulations with various stratification regimes that could then serve as references or constraints for ITs corrections atlases. This approach should be preferably used for regions where the stratification regime can set, as in the mid-latitudes areas with weak circulation. However, for regions with highly variable stratification regimes and strong circulation, this approach should be used with caution. Such modeling would not be representative of the circulation and also could be highly unstable.

Finally, coupling the two approaches of clustering methods and the academic simulations results in the production of two types of climatologies of the ITs amplitudes and wavelengths for the five first baroclinic modes. For the western equatorial Atlantic, the wavelengths can be linearly derived from the pycnocline depth for a constant bathymetry. Whereas in the Bay of Biscay, the wavelengths have to be determined progressively during the year. The clustering methods enable us to set the delimitation of the seasons based on the stratification rather than on monthly climatologies. The efforts to find a formulation to link the ITs amplitude and wavelengths to the stratification need to be pursued for the mid-latitudes in order to obtain a parametrization that could unify the different regions of the global ocean.

Currently, the SWOT mission encourages international efforts in order to separate the mesoscale and ITs' surface elevation contributions. This study invites other researchers to carefully consider the background stratification and even more its variability within the different approaches used, in order to predict and remove the ITs' surface elevation signature.

Code and data availability. The hydrodynamic code T-UGOm (CECILL licence) is available at https://hg.legos.obs-mip.fr/tugo Mercurial repository. The climatologies of the ITWs properties in the Bay of Biscay are available upon request to the authors.

Author contributions. SB developed the clustering methodology, ran the simulations and realised all the graphics and interpretations. FL developed T-UGOm, built the model configuration for previous studies and supervised the runs. FL, MT and LC enhanced the interpretations and graphics with their relevant advises.

Competing interests. No competing interest to declare.

Acknowledgements. The authors are grateful to the CNES, CLS, CNRS and UPS for the funding of this study as well as the projects COCTO (PIs: N. Ayoub and P. De Mey-Frémaux) and HighFreq (PI: F. Lyard) for the additional funding of diverse missions for the communication of this study. D. Allain is also thanked for his help for the simulations and the development of POCViP. The developers of Scikit-learn Python package (Pedregosa et al., 2011) are thanked for providing a well-documented package on machine learning algorithms. Rosemary Morrow is thanked for her helpful comments about the smooth understanding and the writing of this article.

References

Arbic, B. K., Lyard, F., Ponte, A., Ray, R. D., Richman, J. G., Shriver, J. F., Zaron, E., and Zhao, Z.: Tides and the SWOT mission: Transition from science definition team to science team, Civil and Environmental Engineering Faculty Publications and Presentations, 336, 2015.

Carrere, L., Le Provost, C., and Lyard, F.: On the statistical stability of the M2 barotropic and baroclinic tidal characteristics from along-track TOPEX/Poseidon satellite altimetry analysis, Journal of Geophysical Research: Oceans, 109, 2004.

Carrere, L., Arbic, B. K., Dushaw, B., Egbert, G., Erofeeva, S., Lyard, F., Ray, R. D., Ubelmann, C., Zaron, E., Zhao, Z., et al.: Accuracy assessment of global internal-tide models using satellite altimetry, Ocean Science, 17, 147–180, 2021.

Charraudeau, R. and Vandermeirsch, F.: Bay of Biscay's temperature and salinity climatology, Tech. rep., Ifremer, http://www.ifremer.fr/climatologie-gascogne/reference/summary_sea_tech_we.pdf, 2006.

Chuang, W.-S. and Wang, D.-P.: Effects of density front on the generation and propagation of internal tides, Journal of Physical Oceanography, 11, 1357–1374, 1981.

Duda, T. F., Lin, Y.-T., Buijsman, M., and Newhall, A. E.: Internal Tidal modal ray refraction and energy ducting in baroclinic Gulf Stream currents, Journal of Physical Oceanography, 48, 1969–1993, 2018.

Feistel, R.: A new extended Gibbs thermodynamic potential of seawater, Progress in Oceanography, 58, 43–114, 2003.

Feistel, R.: A Gibbs function for seawater thermodynamics for- 6 to 80 C and salinity up to 120 g kg–1, Deep Sea Research Part I: Oceanographic Research Papers, 55, 1639–1671, 2008.

Ffield, A.: North Brazil current rings viewed by TRMM Microwave Imager SST and the influence of the Amazon Plume, Deep Sea Research Part I: Oceanographic Research Papers, 52, 137–160, 2005.

Fu, L.-L. and Ubelmann, C.: On the transition from profile altimeter to swath altimeter for observing global ocean surface topography, Journal of Atmospheric and Oceanic Technology, 31, 560–568, 2014.

Gaillard, F.: ISAS-13-CLIM temperature and salinity gridded climatology, https://doi.org/10.17882/45946, 2015.

Garraffo, Z. D., Johns, W. E., Chassignet, E. P., and Goni, G. J.: North Brazil Current rings and transport of southern waters in a high resolution numerical simulation of the North Atlantic, in: Elsevier Oceanography Series, vol. 68, pp. 375–409, Elsevier, 2003.

Garzoli, S. L., Ffield, A., Johns, W. E., and Yao, Q.: North Brazil Current retroflection and transports, Journal of Geophysical Research: Oceans, 109, 2004.

Gill, A.: Atmospheric-ocean dynamics, vol. 30, Academic press, 1982.

Goni, G. J. and Johns, W. E.: Synoptic study of warm rings in the North Brazil Current retroflection region using satellite altimetry, in: Elsevier Oceanography Series, vol. 68, pp. 335–356, Elsevier, 2003.

Gustafsson, F.: Determining the initial states in forward-backward filtering, IEEE Transactions on Signal Processing, 44, 988–992, https://doi.org/10.1109/78.492552, 1996.

Hjelmervik, K. and Hjelmervik, K. T.: Time-calibrated estimates of oceanographic profiles using empirical orthogonal functions and clustering, Ocean Dynamics, 64, 655–665, https://doi.org/10.1007/s10236-014-0704-y, 2014.

Hjelmervik, K. T. and Hjelmervik, K.: Estimating temperature and salinity profiles using empirical orthogonal functions and clustering on historical measurements, Ocean Dynamics, 63, 809–821, https://doi.org/10.1007/s10236-013-0623-3, 2013.

Irwin, A. J. and Oliver, M. J.: Are ocean deserts getting larger?, Geophysical Research Letters, 36, https://doi.org/10.1029/2009GL039883, 2009.

Johns, W. E., Lee, T., Beardsley, R., Candela, J., Limeburner, R., and Castro, B.: Annual cycle and variability of the North Brazil Current, Journal of Physical Oceanography, 28, 103–128, 1998.

Kundu, P., Cohen, M. I., and Hu, H. H.: Fluid mechanics, Elsevier Academic Press, Amsterdam, 2004.

Le Bars, Y., Lyard, F., Jeandel, C., and Dardengo, L.: The AMANDES tidal model for the Amazon estuary and shelf, Ocean Modelling, 31, 132–149, 2010.

Lyard, F., Allain, D., Cancet, M., Carrere, L., and Picot, N.: FES2014 global ocean tide atlas: design and performance, Ocean Science, 7, 190–240, 2021.

Magalhães, J. M., Da Silva, J., Buijsman, M. C., and Garcia, C.: Effect of the North Equatorial Counter Current on the generation and propagation of internal solitary waves off the Amazon shelf (SAR observations), Ocean Science, 12, 243–255, 2016.

Marsaleix, P., Auclair, F., Floor, J. W., Herrmann, M. J., Estournel, C., Pairaud, I., and Ulses, C.: Energy conservation issues in sigma-coordinate free-surface ocean models, Ocean Modelling, 20, 61–89, 2008.

Martin Traykovski, L. V. and Sosik, H. M.: Feature-based classification of optical water types in the Northwest Atlantic based on satellite ocean color data, Journal of Geophysical Research: Oceans, 108, https://doi.org/10.1029/2001JC001172, 2003.

Millero, F. J., Feistel, R., Wright, D. G., and McDougall, T. J.: The composition of Standard Seawater and the definition of the Reference-Composition Salinity Scale, Deep Sea Research Part I: Oceanographic Research Papers, 55, 50–72, 2008.

Morrow, R., Fu, L.-L., Ardhuin, F., Benkiran, M., Chapron, B., Cosme, E., d'Ovidio, F., Farrar, J. T., Gille, S. T., Lapeyre, G., et al.: Global observations of fine-scale ocean surface topography with the Surface Water and Ocean Topography (SWOT) mission, Frontiers in Marine Science, 6, 232, 2019.

Nugroho, D.: The tides in a general circulation model in the Indonesian seas, Ocean, Atmosphere. Université Paul Sabatier - Toulouse III, https://tel.archives-ouvertes.fr/tel-01897523/document, english. NT: 2017TOU30089. tel-01897523, 2017.

Oliver, M. J., Glenn, S., Kohut, J. T., Irwin, A. J., Schofield, O. M., Moline, M. A., and Bissett, W. P.: Bioinformatic approaches for objective detection of water masses on continental shelves, Journal of Geophysical Research: Oceans, 109, https://doi.org/10.1029/2003JC002072, 2004.

Pairaud, I. L., Auclair, F., Marsaleix, P., Lyard, F., and Pichon, A.: Dynamics of the semi-diurnal and quarter-diurnal internal tides in the Bay of Biscay. Part 2: Baroclinic tides, Continental Shelf Research, 30, 253–269, 2010.

Pauthenet, E., Roquet, F., Madec, G., Guinet, C., Hindell, M., McMahon, C. R., Harcourt, R., and Nerini, D.: Seasonal Meandering of the Polar Front Upstream of the Kerguelen Plateau, Geophysical Research Letters, 45, 9774–9781, https://doi.org/10.1029/2018GL079614, 2018.

Pedregosa, F., Varoquaux, G., Gramfort, A., Michel, V., Thirion, B., Grisel, O., Blondel, M., Prettenhofer, P., Weiss, R., Dubourg, V., Vanderplas, J., Passos, A., Cournapeau, D., Brucher, M., Perrot, M., and Duchesnay, E.: Scikit-learn: Machine Learning in Python, Journal of Machine Learning Research, 12, 2825–2830, 2011.

Pegliasco, C., Chaigneau, A., and Morrow, R.: Main eddy vertical structures observed in the four major Eastern Boundary Upwelling Systems, Journal of Geophysical Research: Oceans, 120, 6008–6033, 2015.

Pereira, A., Castro, B., Calado, L., and da Silveira, I.: Numerical simulation of M2 internal tides in the South Brazil Bight and their interaction with the Brazil Current, Journal of Geophysical Research: Oceans, 112, 2007.

Pichon, A. and Correard, S.: Internal tides modelling in the Bay of Biscay. Comparisons with observations, Scientia Marina, 70, 65–88, 2006.

Pichon, A. and Maze, R.: Internal Tides over a Shelf Break: Analytical Model And Observations, American Meteorological Society, pp. 657–671, 1990.

Piton, V., Herrmann, M., Lyard, F., Marsaleix, P., Duhaut, T., Allain, D., and Ouillon, S.: Sensitivity study on the main tidal constituents of the Gulf of Tonkin by using the frequency-domain tidal solver in T-UGOm., Geoscientific Model Development, 13, 2020.

Ponte, A. L. and Klein, P.: Incoherent signature of internal tides on sea level in idealized numerical simulations, Geophysical Research Letters, 42, 1520–1526, 2015.

Ray, R. D. and Mitchum, G. T.: Surface manifestation of internal tides generated near Hawaii, Geophysical Research Letters, 23, 2101–2104, 1996.

Ray, R. D. and Mitchum, G. T.: Surface manifestation of internal tides in the deep ocean: Observations from altimetry and island gauges, Progress in Oceanography, 40, 135–162, 1997.

Ray, R. D. and Zaron, E. D.: M2 Internal Tides and Their Observed Wavenumber Spectra from Satellite Altimetry, Journal of Physical Oceanography, 46, 3–22, https://doi.org/10.1175/JPO-D-15-0065.1, 2016.

Richardson, P. and Reverdin, G.: Seasonal cycle of velocity in the Atlantic North Equatorial Countercurrent as measured by surface drifters, current meters, and ship drifts, Journal of Geophysical Research: Oceans, 92, 3691–3708, 1987.

Ruault, V., Jouanno, J., Durand, F., Chanut, J., and Benshila, R.: Role of the tide on the structure of the Amazon plume: a numerical modeling approach, Journal of Geophysical Research: Oceans, 125, e2019JC015 495, 2020.

Sokal, R. R.: A statistical method for evaluating systematic relationships, Univ. Kansas, Sci. Bull., 38, 1409–1438, 1958.

Soufflet, Y., Marchesiello, P., Lemarié, F., Jouanno, J., Capet, X., Debreu, L., and Benshila, R.: On effective resolution in ocean models, Ocean Modelling, 98, 36–50, 2016.

Szekely, T., Gourrion, J., Pouliquen, S., and Reverdin, G.: CORA, Coriolis Ocean Dataset for Reanalysis, https://doi.org/10.17882/46219, 2016.

Tchilibou, M., Gourdeau, L., Lyard, F., Morrow, R., Koch Larrouy, A., Allain, D., and Djath, B.: Internal tides in the Solomon Sea in contrasted ENSO conditions, Ocean Science Discussions, 2019, 1–40, https://doi.org/10.5194/os-2019-94, 2019.

Von Luxburg, U.: A Tutorial on Spectral Clustering, https://doi.org/10.1.1.165.9323, 2007.

Ward, J. J. H.: Hierarchical grouping to maximize payoff, Tech. rep., PERSONNEL RESEARCH LAB LACKLAND AFB TX, 1961.

Ward, J. J. H. and Hook, M. E.: Application of an hierarchical grouping procedure to a problem of grouping profiles, Educational and Psychological Measurement, 23, 69–81, 1963.

Welch, P.: The use of fast Fourier transform for the estimation of power spectra: a method based on time averaging over short, modified periodograms, IEEE Transactions on audio and electroacoustics, 15, 70–73, 1967.

Yu, S. X. and Shi, J.: Multiclass Spectral Clustering, International Conference on Computer Vision, Nice, France, 11-17 Oct 2003, https://www1.icsi.berkeley.edu/~stellayu/publication/doc/2003kwayICCV.pdf, 2003.

Zaron, E. D.: Baroclinic Tidal Sea Level from Exact-Repeat Mission Altimetry, Journal of Physical Oceanography, 49, 193–210, https://doi.org/10.1175/JPO-D-18-0127.1, 2019.

Zaron, E. D. and Ray, R. D.: Using an altimeter-derived internal tide model to remove tides from in situ data, Geophysical Research Letters, 44, 4241–4245, 2017.

Zhao, Z., Wang, J., Fu, L.-L., Chen, S., Qiu, B., and Menemenlis, D.: Mapping Internal Tides using Synthetic SWOT Measurements, in: AGU Fall Meeting Abstracts, 2018.

Zhao, Z., Wang, J., Menemenlis, D., Fu, L.-L., Chen, S., and Qiu, B.: Decomposition of the multimodal multidirectional M2 internal tide field, Journal of Atmospheric and Oceanic Technology, 36, 1157–1173, 2019.

Appendix A: Tests to set the best parameters and methods for the clustering

815   Three different methods of clustering have been tested: Ward, Average and Spectral (Python SciKitLearn clustering package[9]). Those methods have been selected because they can better classify the distribution of the PCA manifold (Fig. A1). The Average hierarchical clustering method builds the complete tree that links the points by minimizing the average of the distances between the clusters being merged in order to build the tree (WPGMA, Sokal, 1958). The Ward hierarchical clustering method is based on the same methodology as Average but minimizes the variance of the clusters being merged (Ward, 1961; Ward and Hook,

820   1963). The Spectral clustering method is different from the previous two. This method projects the PCA manifold onto a polar coordinate space before performing the classification through a specified number of clusters and minimizing the distance within each cluster (Yu and Shi, 2003; Von Luxburg, 2007).

    For these three methods, the sensitivity of two parameters needs to be investigated: the number of final clusters and the number of neighbors used in the calculation of the distance between profiles. The number of neighbors is important to properly

825   manage the profiles that are isolated outside the PCA manifold. If the number of neighbors is weaker than the number of outsider profiles, then they all will be grouped in a dedicated cluster. Otherwise, they will be included in the cluster of the nearest profiles. This latter case can lead to groups of profiles that do not have the same shape inside the same cluster. The number of neighbors also affects the profiles located at the boundary between two clusters: depending on the number of neighbors, they will be included in one cluster or another. This last parameter is the first to be tested with a value of 4, 8, 12

830   and 16 over the three clustering methods.

    Figure A2 shows the sensitivity of the clustering methods to the considered number of neighbors. First, the Average method gathers almost all the profiles in one cluster so it seems irrelevant for the classification. Second, the sensitivity to this parameter

---

[9]https://scikit-learn.org/stable/modules/clustering.html
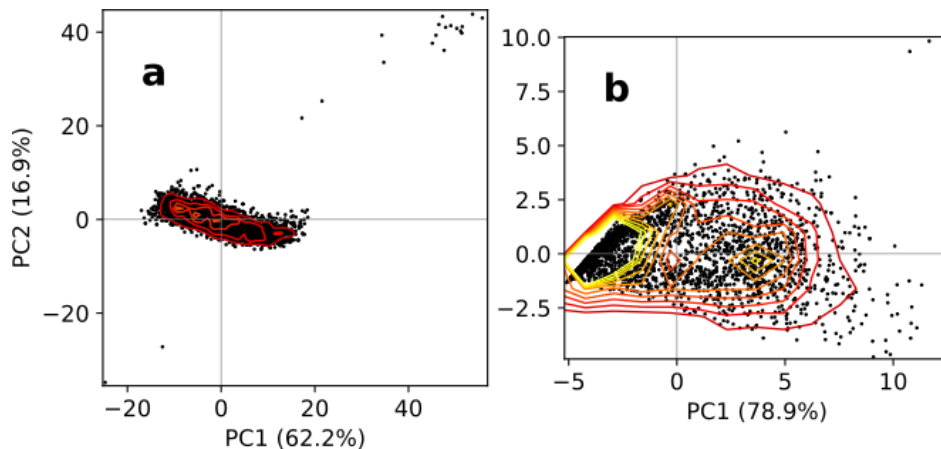
Figure A1. PCA manifold for (a) the western equatorial Atlantic and (b) the Bay of Biscay. The colored contours correspond to the density of points from 10 to 100 by tens.
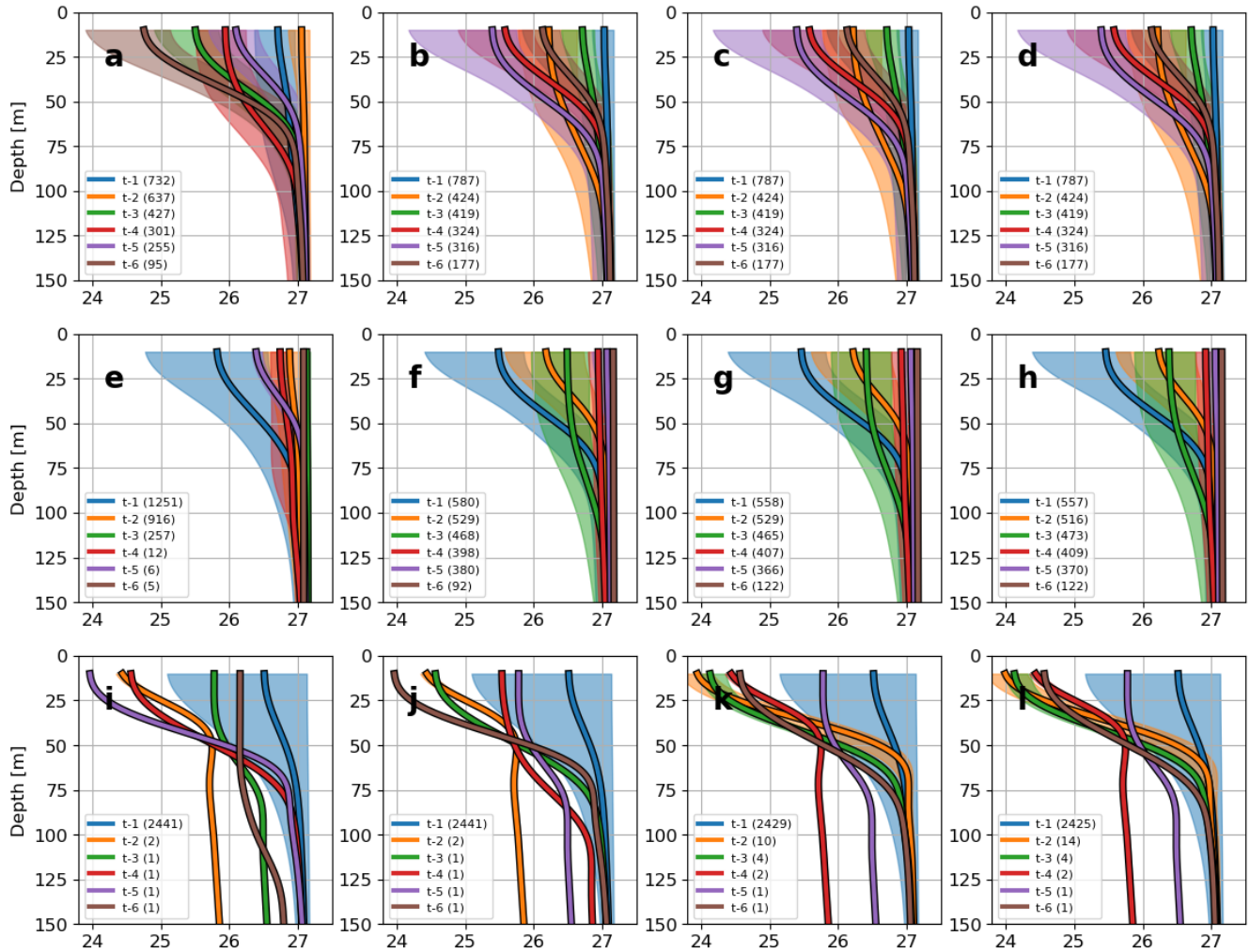
Figure A2. Clustering of the density profiles of the Bay of Biscay for (a-d) Ward, (e-h) Spectral and (i-l) Average methods. For each method, the calculation is made considering (a,e,i) 4 neighbors, (b,f,j) 8 neighbors, (c,g,k) 12 neighbors and (d,h,l) 16 neighbors. The number of profiles inside each cluster is given in the legend between brackets.

is very low for the Ward and Average methods but larger for the Spectral method. The classifications using the 16 nearest neighbors are distributed more equally between the clusters. Thus, for the following investigation, the Ward method is tested with 16 neighbors. For both areas, the classification is made for 2 to 10 clusters.

Figures A3 and A4 illustrate the different classifications made using different numbers of clusters. For the western equatorial Atlantic, the variability of the density profiles is mainly controlled by the pycnocline depth. For 3 to 7 clusters, a unique cluster gathers suspicious profiles that seem to have an offset problem. For 8 to 9 clusters, the new clusters describe the different sets of suspicious profiles. For 10 clusters, the new cluster describe the main variability of the density profiles. The clusters of clean data are very similar and the increase of the number of cluster only increase the number of pycnocline depth described. Thus, a few clusters can describe the full variability of the density profiles. For the Bay of Biscay, every cluster describes a different type of density profiles that has different surface density and different N profile. But for 7 to 10 clusters, some clusters only describe a few profiles: less than 100 profiles over around 15 years of data, which questions the significance of these clusters.
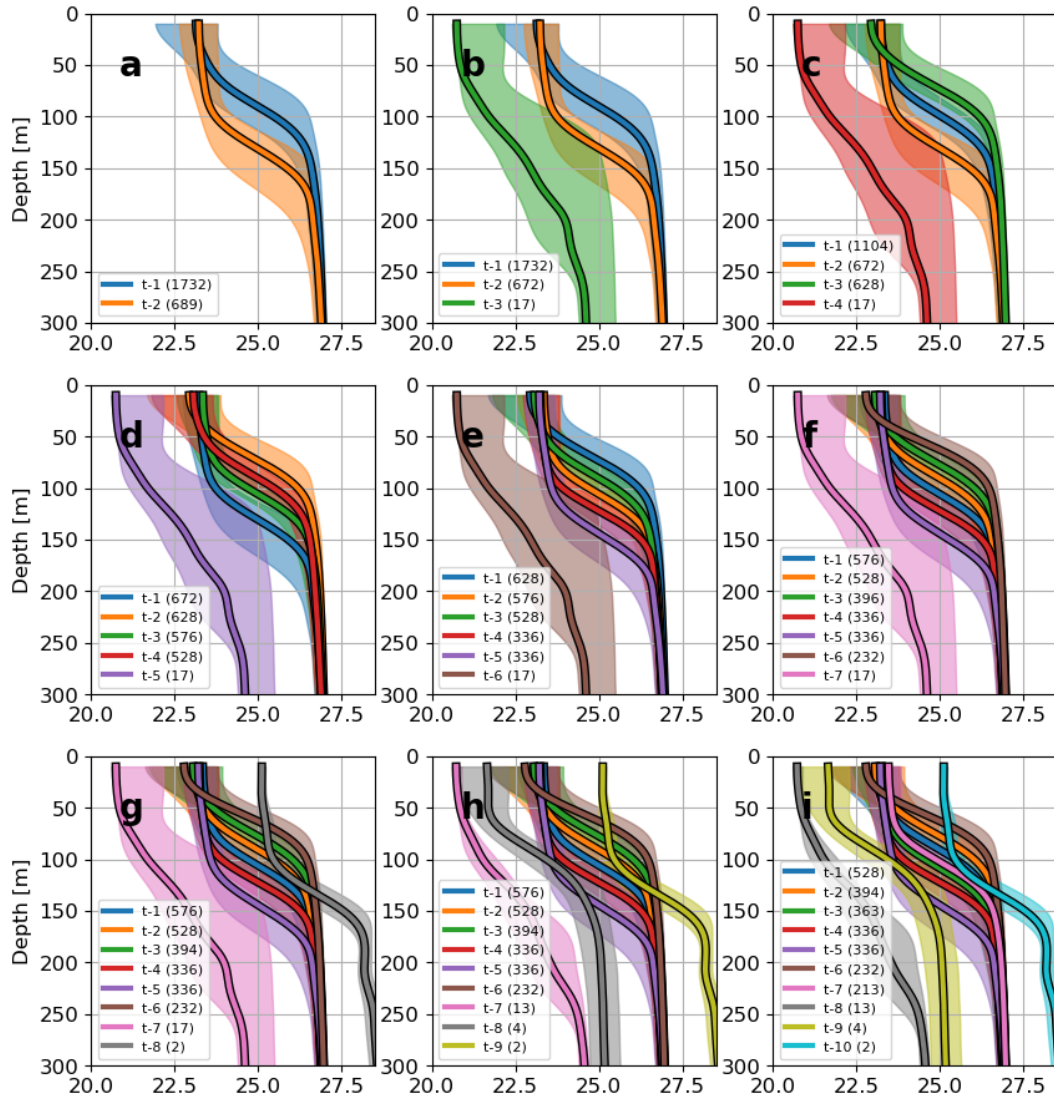
Figure A3. Ward clustering of the density profiles of the western equatorial Atlantic for a different number of clusters, from 2 to 10. The number of profiles inside each cluster is given in the legend between brackets.
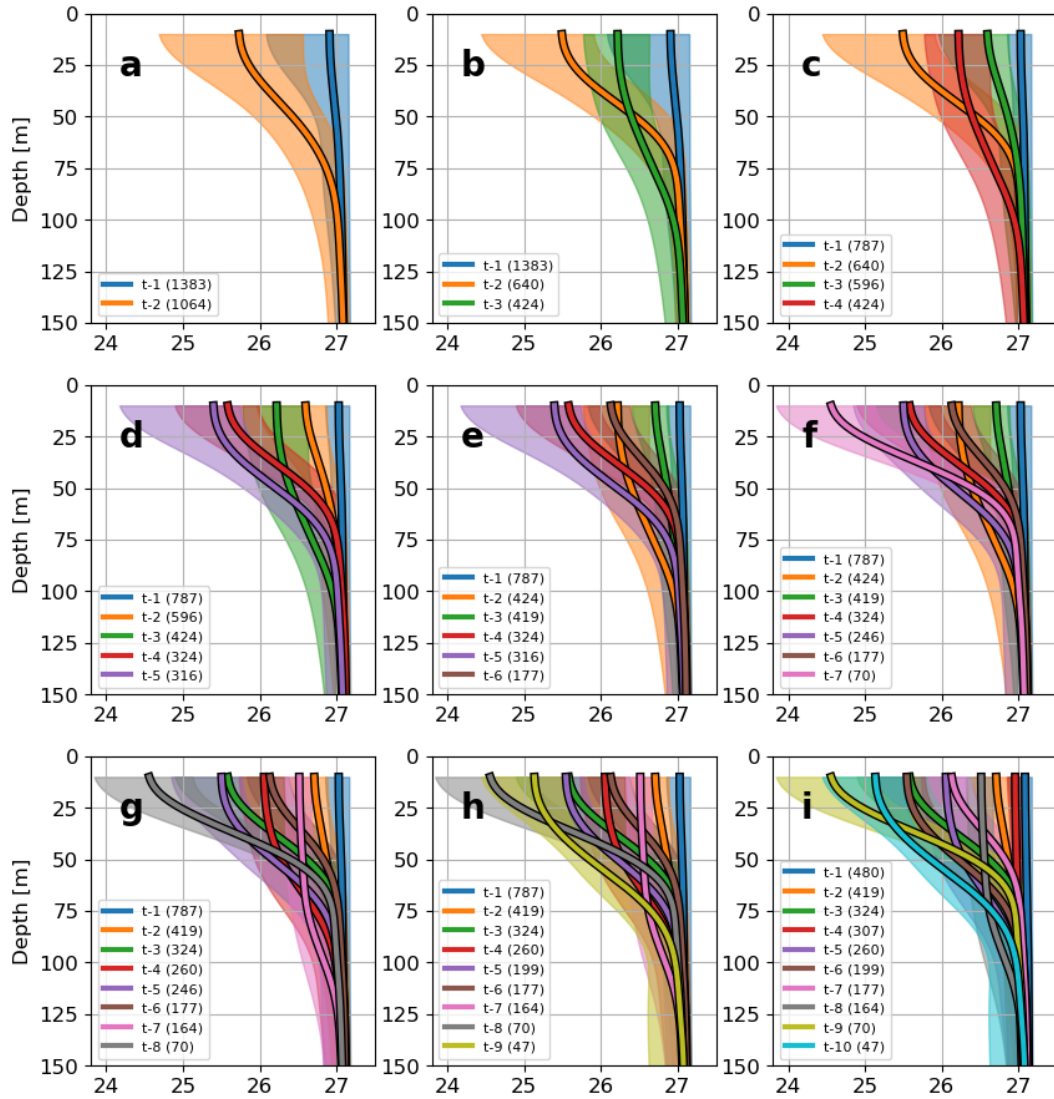
Figure A4. Ward clustering of the density profiles of the Bay of Biscay for a different number of clusters, from 2 to 10. The number of profiles inside each cluster is given in the legend between brackets.

Appendix B: western equatorial Atlantic additional visualization of the clusters
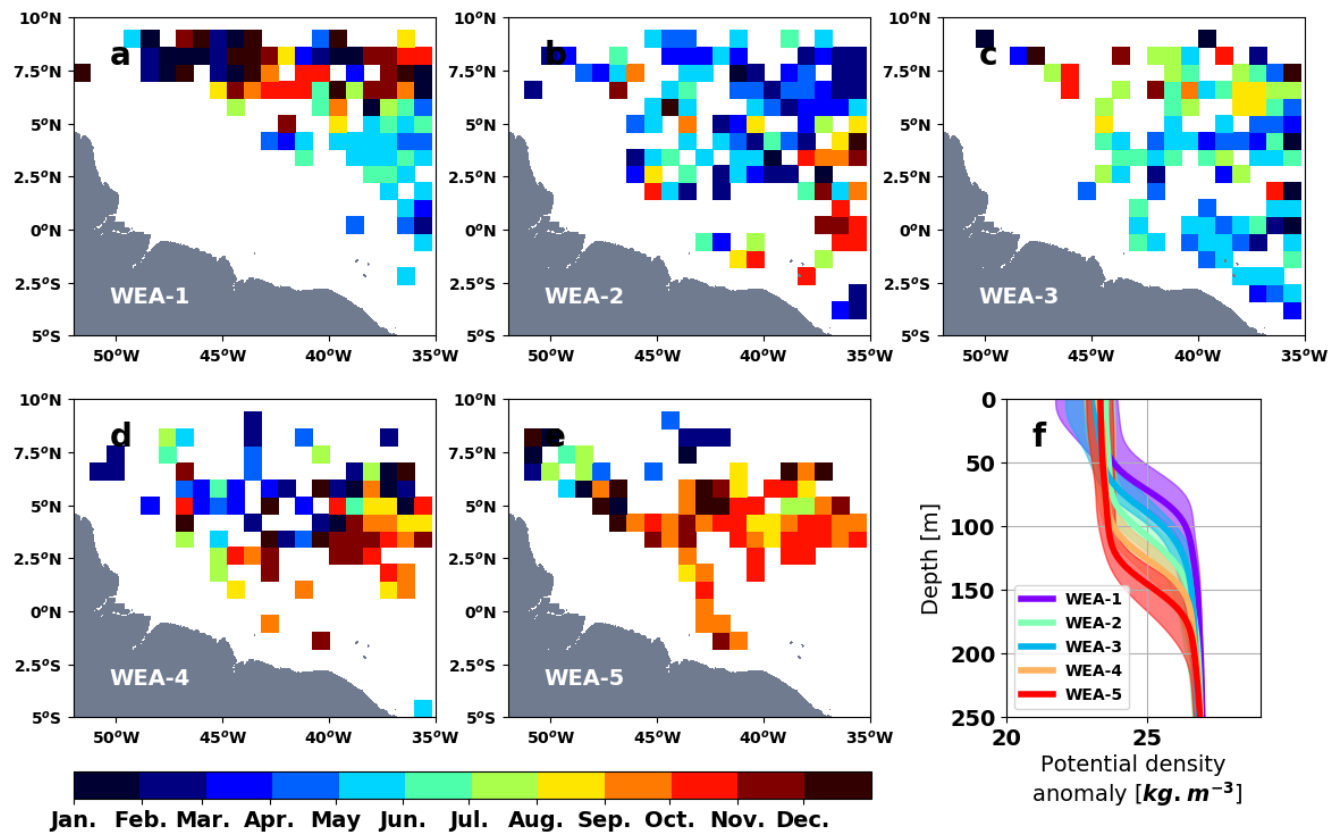
Figure B1. (a-e) Mean seasonality over the area for each cluster in the western equatorial Atlantic and (f) the median profiles of the clusters from the figure 3. The mean season is processed over the area within boxes of 1x1 degree, only the boxes with more than 2 profiles are showed.

   Appendix C: Bathymetry used in the COMODO configuration
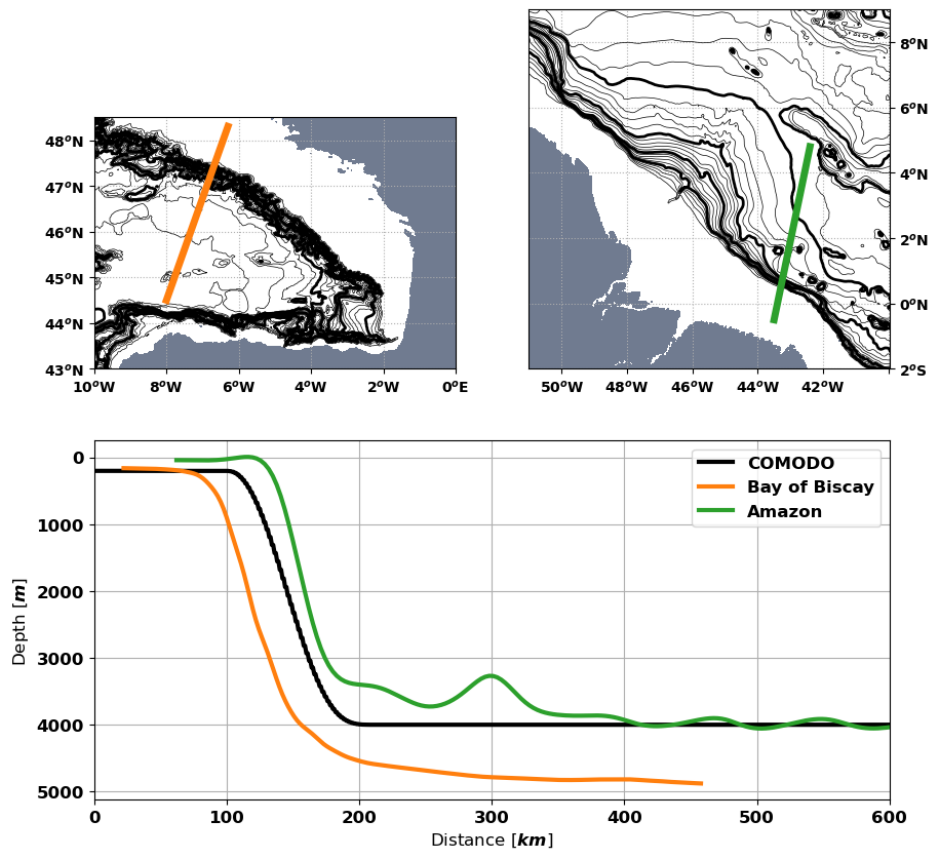
Figure C1. Realistic continental slope bathymetry over the two studied area compared to the COMODO one.